UNIVERSIDADE FEDERAL DO CEARÁ
CENTRO DE TECNOLOGIA
DEPARTAMENTO DE ENGENHARIA QUÍMICA
PROGRAMA DE PÓS-GRADUAÇÃO EM ENGENHARIA QUÍMICA

EVELYN CLAUDIA QUINTEROS SORIA

EXPERIMENTAL DETERMINATION AND THERMODYNAMIC MODELING OF PHASE EQUILIBRIUM IN SYSTEMS WITH CO_2 + DECANE + HEXADECANE

FORTALEZA
2025

EVELYN CLAUDIA QUINTEROS SORIA

EXPERIMENTAL DETERMINATION AND THERMODYNAMIC MODELING OF PHASE EQUILIBRIUM IN SYSTEMS WITH CO_2 + DECANE + HEXADECANE.

Dissertação de Mestrado presentado ao Programa de Pós-Graduação em Engenharia Química, da Universidade Federal do Ceará, como requisito parcial à obtenção do título de Mestre em Engenharia Química. Área de concentração: Processos Químicos e Bioquímicos.

Orientador: Prof. Dr. Filipe Xavier Feitosa.
Coorientador: Prof. Dr. Hosiberto Batista de Sant'Ana.

FORTALEZA
2025

Dados Internacionais de Catalogação na Publicação
Universidade Federal do Ceará
Sistema de Bibliotecas
Gerada automaticamente pelo módulo Catalog, mediante os dados fornecidos pelo(a) autor(a)

S691e Soria, Evelyn Claudia Quinteros.
Experimental determination and thermodynamic modeling of phase equilibrium in systems with CO2 + decane + hexadecane / Evelyn Claudia Quinteros Soria. – 2025.
83 f. : il. color.

Dissertação (mestrado) – Universidade Federal do Ceará, Centro de Tecnologia, Programa de Pós-Graduação em Engenharia Química, Fortaleza, 2025.
Orientação: Prof. Dr. Filipe Xavier Feitosa.
Coorientação: Prof. Dr. Hosiberto Batista de Sant'Ana.

1. Flow assurance. 2. Barotropic inversion. 3. Vapor-liquid equilibria. 4. Liquid-liquid equilibria. 5. Vapor-liquid-liquid equilibria. I. Título.

CDD 660

EVELYN CLAUDIA QUINTEROS SORIA

EXPERIMENTAL DETERMINATION AND THERMODYNAMIC MODELING OF PHASE EQUILIBRIUM IN SYSTEMS WITH CO_2 + DECANE + HEXADECANE.

Dissertação submetida à Coordenação do curso de pós-graduação em Engenharia Química da Universidade Federal do Ceará, como requisito parcial para a obtenção do grau de Mestre em Engenharia Química.

Aprovada em: 06/01/2025.

BANCA EXAMINADORA

Prof. Dr. Filipe Xavier Feitosa (Orientador)
Universidade Federal do Ceará (UFC)

Prof. Dr. Moisés Bastos Neto
Universidade Federal do Ceará (UFC)

Prof. Dr. Frederico Ribeiro Do Carmo
Iniversidade Federal Rural do Semi-Árido (UFERSA)

ACKNOWLEDGMENTS

To God, for supporting me throughout my journey. To my guardian angel, my mother Conzuelo Soria, whose memory is the promise I made to continue and advance with my Master's degree. To my family, for motivating me to take on this challenge and for their unwavering support: my father Johnny Quinteros and my sisters Andrea and Daniela.

To Prof. Dr. Filipe Xavier Feitosa and Prof. Dr. Hosiberto Batista de Sant'Ana, for their excellent guidance, teaching, and support throughout this program.

To my GPTA friends.

And a special thank you to my friends from other countries whom I met in Brazil, who left me with valuable memories and lessons.

RESUMO

O comportamento de fases dos fluidos de reservatório é crucial para avaliar a viabilidade do desenvolvimento de um campo de petróleo. As variações de pressão, temperatura e composição durante a produção podem desencadear transições de fases complexas que afetam o escoamento. Um dos desafios inerentes ao estudo do comportamento de fases dos fluidos de reservatório está relacionado à sua opacidade e à evidente complexidade de determinar dados de equilíbrio de fases devido às suas características intrínsecas. Por esse motivo, sistemas modelo são utilizados para representar comportamentos específicos por meio de componentes chave. Este estudo apresenta dados experimentais de equilíbrio de fases e modelagem termodinâmica para o sistema ternário dióxido de carbono + decano + hexadecano em temperaturas de T = (283,15, 298,15 e 323,15) K e pressões de até 20 MPa. Essas temperaturas foram escolhidas para cobrir condições tanto subcríticas quanto supercríticas para o dióxido de carbono (CO_2). Especificamente, o CO_2 é subcrítico a 283,15 K e 298,15 K e supercrítico a 323,15 K, dada sua temperatura crítica de 304,21 K. Os experimentos foram realizados utilizando diferentes proporções de hexadecano na mistura binária (hexadecano/decano), ou seja, 20%, 40%, 60% e 80% de fração molar da mistura líquida, para avaliar seu impacto no comportamento de fases. O equilíbrio vapor-líquido foi observado para os sistemas ternários com até 40% de hexadecano na mistura líquida de hidrocarbonetos a 298,15 K. Para condições de temperatura subcrítica, o equilíbrio líquido-líquido foi identificado a partir dessa composição. A 323 K, pontos de orvalho foram observados em frações molares de CO_2 superiores a 90%. No entanto, a complexidade aumenta quando a composição molar de hexadecano atinge 60% ou mais na mistura binária de hidrocarbonetos líquidos. Nessas condições, foram observadas transições de fases de líquido para líquido-líquido e de líquido-líquido para líquido-líquido-vapor, juntamente com o fenômeno de inversão barotrópica, a uma temperatura de 298,15 K. A equação de estado de Peng-Robinson foi utilizada para modelar os pontos experimentais, com os parâmetros de interação binária para os pares de componentes sendo obtidos: o par CO_2/decano foi determinado por regressão de dados experimentais deste trabalho, enquanto o par CO_2/hexadecano foi derivado por regressão de dados da literatura. Os resultados revelam comportamentos complexos à medida que a composição de hexadecano na mistura aumenta. Este estudo fornece dados valiosos sobre sistemas modelo que representam o petróleo bruto, destacando comportamentos complexos em sistemas ternários com alto teor de dióxido de carbono.

Palavras-chave: garantia de escoamento; fluidos de reservatório; equilíbrio liquido-vapor; equilíbrio liquido-liquido; equilíbrio liquido-liquido-vapor; inversão barotrópica.

ABSTRACT

The phase behavior of reservoir fluids is crucial for evaluating the feasibility of oilfield development. Variations in pressure, temperature, and composition during production can trigger complex phase transitions that affect flow. One of the inherent challenges in studying the phase behavior of reservoir fluids is related to their opacity and the evident complexity of determining phase equilibrium data due to their intrinsic characteristics. For this reason, model systems are used to represent specific behaviors through key components. This study presents experimental phase equilibrium data and thermodynamic modeling for the carbon dioxide + decane + hexadecane ternary system at temperatures of T = (283.15, 298.15, and 323.15) K and pressures up to 20 MPa. These temperatures were chosen to cover both subcritical and supercritical conditions for carbon dioxide (CO_2). Specifically, CO_2 is subcritical at 283.15 K and 298.15 K, and supercritical at 323.15 K, given its critical temperature of 304.21 K. The experiments were carried out using different proportions of hexadecane in the binary mixture (hexadecane/decane), i.e., 20%, 40%, 60%, and 80% molar fraction of the liquid mixture, to its impact evaluate on phase behavior. Vapor-liquid equilibrium was observed for the ternary systems with up to 40% hexadecane in the hydrocarbon liquid mixture at 298.15 K. For subcritical temperature conditions, liquid-liquid equilibrium was observed starting from this composition. At 323,15 K, dew points were observed at CO_2 mole fractions greater than 90%. However, complexity arises when the molar composition of hexadecane reaches 60% or higher in the binary liquid hydrocarbon mixture. Under these conditions, phase transitions from liquid to liquid-liquid and from liquid-liquid to vapor-liquid-liquid were observed, along with the barotropic inversion phenomenon, at a temperature of 298.15 K. The Peng-Robinson equation of state was used to model the experimental points, with binary interaction parameters for the component pairs being obtained: the CO_2/decane pair was obtained by regression of experimental data of this work, while the CO_2/hexadecane pair was determined through regression of literature data. The results reveal complex behaviors as the hexadecane composition in the mixture increases. This study provides valuable data on model systems representing crude oil, highlighting complex behaviors in ternary systems with high carbon dioxide content.

Keywords: flow assurance; reservoir fluids; vapor-liquid equilibria; liquid-liquid equilibria; vapor-liquid-liquid equilibria; barotropic inversion.

LIST OF FIGURES

LIST OF TABLES

LIST OF ABBREVIATIONS AND ACRONYMS

%AARD	Percentage Absolute Average Deviation
CCE	Constant Composition Expansion
EC	Equilibrium Cell
ELL	Liquid-liquid equilibria
ELLV	Vapor-liquid-liquid equilibria
ELV	Vapor-liquid equilibria
EOR	Enhanced Oil Recovery
EOS	Equation of State
GOR	Gas-oil ratio
LCEP	Lower Critical End Point
LV	Liquid-Vapor
LLV	Liquid-liquid-vapor
MaDI	Mass Density Inversion
MoDI	Molar Density Inversion
OF	Objective Function
PR	Peng Robinson
PVT	Pressure-Volume-Temperature
UCEL	Upper Critical Line
UCEP	Upper Critical End Point
VdW	Van der Walls

LIST OF SYMBOLS

a	Attractive parameter of the VdW equation
b	Co-volume used in the VdW equation
f	Fugacity
$\mathbf{k_{ij}}$	Binary interaction parameter
Np	Number of components
P	Pressure
R	Universal gas constant
T	Temperature
x	Mole fraction
Z	Compressibility factor
$\boldsymbol{\omega_i}$	Acentric Factor
μ	Chemical Potential

SUMMARY

1 INTRODUCTION

The characterization of the phases that can arise due to variations in pressure, temperature and composition during oil production has represented a challenge in recent years. This objective has generated a growing interest in the design and optimization of processes with the aim of improving efficiency in oil extraction (Savonina; Panyukova, 2023). Understanding this behavior is essential for effective reservoir development and management, as it impacts all aspects of oil exploration and production.

Hydrocarbons in reservoirs can exist in vapor, liquid or solid phases. Each phase represents a distinct region within the system with well-defined boundaries. With variations in temperature and pressure, phases can form, disappear, or change their properties in a multiphase system, reflecting the dynamic nature of reservoir conditions (Ayala H.; Morgan, 2016).

Recent exploitation of Brazil's challenging offshore pre-salt fields has intensified efforts to better characterize crude oils. Various studies using modern chromatographic techniques have revealed a significant amount of paraffins in Brazilian pre-salt oils, which are saturated hydrocarbons that affect the physical and chemical properties of the oils (Vanini *et al.*, 2018).

In 2018, the research group led by Vanini et al. used high-resolution analytical techniques to achieve a detailed characterization of crude oils from Brazil. Their analysis indicated that the main compound classes include paraffins, with n-paraffins (linear chains) being more abundant than isoparaffins (branched chains), followed by olefins (alkenes), naphthenes, and aromatics (Vanini *et al.*, 2018). This composition not only highlights chemical diversity, which includes high- and low-molecular-weight compounds, but also a high carbon dioxide (CO_2) content, which directly influences the phase behavior of the fluids. Therefore, model systems are used to represent these compounds adequately, aiming to describe and predict phenomena occurring during extraction, separation, enhanced hydrocarbon recovery, and CO_2 capture and storage (Beltrao *et al.*, 2009; Braga; Tavares; Ndiaye, 2022; Edwards; Isacsson, 2005; França *et al.*, 2018; Medeiros *et al.*, 2023).

Research on model systems is essential for designing production methods, optimizing processes, and understanding phase behavior in complex reservoir conditions (Braga; Tavares; Ndiaye, 2022). These systems, also known as blank systems due to the transparency of some compounds, are widely used to determine multiphase equilibrium in reservoir fluids with high gas-oil ratio (GOR) and significant CO_2 content. While reservoir

fluids contain numerous compounds, the basic principles of phase behavior can be understood by studying simplified mixtures with a few components. However, it is important to note that, while model systems provide valuable insights, they may not fully capture the complexities and interactions present in reservoir fluids, particularly those with high CO_2 content and diverse chemical compositions, as found in Brazil's pre-salt reservoirs.

Numerous Enhanced Oil Recovery (EOR) methods are employed globally to enhance the recovery of remaining oil reserves. These technologies are typically implemented after water injection to displace oil. Surfactants can be added to the injection water to reduce interfacial tension and improve the recovery of trapped oil by capillary forces. Additional EOR techniques include gas injections (miscible and immiscible), chemical flooding involving the injection of polymers, surfactants and alkalis, and thermal methods such as steam injections, hot water injections, electrical heating and in situ combustion (Al Ghafri, Saif, 2013).

One method for enhanced hydrocarbon recovery is CO_2 injection, which involves increasing reservoir pressure with large amounts of gas (Romero Yanes *et al.*, 2021). This approach offers advantages, including lower costs, non-toxic and non-flammable properties, and partial contributions to reducing atmospheric CO_2 levels. Furthermore, CO_2 shows greater solubility and miscibility with petroleum fluids (Kariznovi; Nourozieh; Abedi, 2013).

The significant quadrupole moment of CO_2 is particularly relevant in studies involving its interactions with other compounds, especially in processes where polarity plays a important role. The disparity in molecular weight compared to n-alkanes reflects an imbalance in size and energy interactions, influencing the thermodynamic behavior of oil and CO_2 mixtures (Cismondi *et al.*, 2012). Due to these unique characteristics, numerous studies on the phase behavior of systems involving CO_2 and various hydrocarbons have been conducted since the 1960s (Kariznovi; Nourozieh; Abedi, 2013). Over the years, many of these studies have become essential to the oil industry (Braga; Tavares; Ndiaye, 2022; Daridon *et al.*, 2021; Eniolorunda; Chapoy; Burgass, 2021; Medeiros *et al.*, 2023; Simoncelli *et al.*, 2020; Yanes; Montel; Daridon, 2022).

A literature review was conducted to assess the availability of data on CO_2 mixtures with decane, n-hexadecane, and other synthetic oils for studying the phase behavior of petroleum fluids. Additionally, the study identified interest in the barotropic inversion phenomenon, observed in systems with high CO_2 content (over 80%) combined with various hydrocarbons, such as n-tetradecane, n-pentadecane, and n-hexadecane (Fall; Fall; Luks, 1985; Nieuwoudt; Du Rand, 2002; Simoncelli *et al.*, 2020). In recent years, understanding and studying this phenomenon has become more relevant due to its potential significance in

reservoir engineering (Flores *et al.*, 2012; Quiñones-Cisneros, 2004; Quinteros-Lama *et al.*, 2015; Tardón *et al.*, 2012).

While abundant research exists on binary CO_2 systems, ternary CO_2 systems still need to be explored. Ternary systems increase the complexity of fluid phase behavior and provide more reliable insights into reservoir scenarios compared to simple binary mixtures. Due to the high complexity of reservoir fluid compositions, a practical approach involves studying ternary mixtures with well-defined compositions (Christov; Dohrn, 2002-; Dohrn *et al.*, 2024; Dohrn; Brunner, 1995). These studies provide valuable information about fluid phase behavior observed in reservoir fluids. This research offers important data on model systems, highlighting complex behaviors in ternary systems with high CO_2 content, especially under temperature conditions near the critical temperature of CO_2. The lack of data on fluid phase equilibria in model systems led to this experimental investigation and modeling of ternary systems.

The objective of this work is to analyze the phase transitions of the ternary system CO_2 + decane + hexadecane at three key temperatures: T = (283.15, 298.15, and 323.15) K. These compounds were selected because decane is widely used to simulate the properties of kerosene and naphtha fractions (Nascimento *et al.*, 2019; Wang *et al.*, 2013). Hexadecane, on the other hand, serves as a representative molecule for studies on barotropic inversion or density changes between two fluid phases under high CO_2 levels and temperatures around 298.15 K (Schneider *et al.*, 1967; Simoncelli *et al.*, 2020). Additionally, hexadecane is used as a reference for the residual liquid phase under atmospheric conditions of petroleum, with a molecular weight ranging between 220-260 g/mol (Hirschberg *et al.*, 1984; Rathmell; Stalkup; Hassinger, 1971; Simoncelli *et al.*, 2020). The three selected temperatures cover both subcritical and supercritical conditions for CO_2. The experiments were conducted using different proportions of hexadecane in the binary mixture (decane + hexadecane), specifically 20%, 40%, 60%, and 80% molar fraction of the liquid mixture, to determine their interactions in phase behavior. The global composition of CO_2 was gradually increased for each of these proportions. From these data, the thermodynamic modeling for studied systems was performed using Peng-Robinson equation of state (Peng; Robinson, 1976) with the van der Waals one-fluid (vdW1f) mixing rules (Kontogeorgis; Folas, 2009).

To accurately identify and study these complex transitions, experimental methods in laboratory environments were employed, specifically PVT (pressure-volume-temperature) experiments. (Fonseca; Dohrn; Peper, 2011) provided a general classification of PVT methods, consisting of two main categories: analytical and synthetic methods. The method used for PVT analysis in this study is the static-synthetic method, defined as a technique in which the global

composition is known, and phase transitions are determined through controlled pressure and temperature changes. This is achieved using microscopy analysis (Braga; Tavares; Ndiaye, 2022; Valero; Maria, 2020). A PVT cell facilitates the investigation of phase transitions by providing precise control of pressure and temperature, along with constant magnetic stirring, allowing phase transitions to be observed through a sapphire window. The Constant Composition Expansion (CCE) technique was employed, where phase transitions were determined using pressure and temperature transmitters, assisted by high-resolution microscopy.

2 OBJECTIVES

In the present work, the following general and specific objectives are to be pursued:

2.1 General objective

Study the phase behavior of the ternary systems composed of n-$C_{10}H_{22}$ + n-$C_{16}H_{34}$ + CO_2 at different temperatures (283.15, 298.15, and 323.15 K) and pressures up to 20 MPa.

2.2 Specific objectives:

I. Determine the phase transitions of the systems by identifying the limits of phase changes in all ternary mixtures at different compositions and temperature conditions. Construct phase diagrams under varying pressures and temperatures using conventional PVT techniques.
II. Identify the occurrence of complex phase equilibria.
III. Study the influence of n-hexadecane on the n-$C_{10}H_{22}$ + n-$C_{16}H_{34}$ + CO_2 ternary system phase transition and the barotropic inversion phenomenon.
IV. Model the phase behavior of the ternary mixtures through basic equation of states.

3 LITERATURE REVIEW

This section presents the main theoretical aspects that comprise the study's objectives, as well the most relevant bibliographic background for the study.

3.1 Phase Equilibria

To understand phase equilibrium, a piston-cylinder setup is schematically illustrated in Figure 1. By varying the volume, thermal and mechanical equilibrium is achieved. These two equilibrium criteria are based on the absence of temperature and pressure gradients, respectively. In this illustration, points α and β can represent any phase: solid, liquid, or vapor and correspond to any of the following equilibria: vapor-liquid, liquid-liquid-solid, gas-solid, liquid-liquid, among others.

Figure 1 - Piston-cylinder scheme

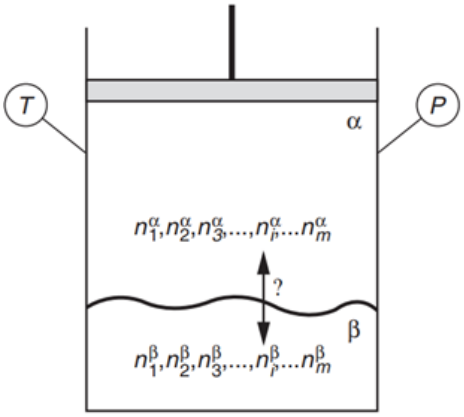

Source: Engineering and Chemical Thermodynamics (2012, p.334).

Consequently, the following definition applies:

$T^{\propto} = T^{\beta}$ Thermal equilibrium (1)

$P^{\propto} = P^{\beta}$ Mechanical equilibrium (2)

These equilibrium criteria are measurable, unlike the thermodynamic property that drives a system toward chemical equilibrium. Its definition is based on the combination of the first and second laws of thermodynamics to develop a property useful to determine whether two phases can coexist in chemical equilibrium (Gibbs, J. Willard, 1874). This property is known as Gibbs energy (G) or Gibbs free energy, mathematically defined as:

$$G = H - TS \qquad (3)$$

Where: H is the enthalpy of the system, T is the absolute temperature and S is the entropy.

Although the Gibbs energy, a derived property, cannot be measured directly, it

provides the same information about chemical equilibrium as temperature does for thermal equilibrium or pressure does for mechanical equilibrium (Koretsky, 2013). As a direct consequence, partial properties are defined for each component within a system. Since the Gibbs energy can be considered a state property, it also meets this definition. In this context, the specific partial property of the Gibbs energy is called the chemical potential, μ, defined as:

$$\mu_i = \left(\frac{\partial G}{\partial n_i}\right)_{T,P,n_{j+i}} \qquad (4)$$

The chemical potential is a derived thermodynamic property, unlike the measured thermodynamic properties, temperature and pressure, which determine thermal and mechanical equilibria. However, its application can be complex due to certain complex mathematical behaviors. To simplify this analysis, fugacity is introduced as a more mathematically manageable derived property, but which preserves the criterion to describe chemical equilibrium.

The definition of fugacity was introduced by Lewis (Lewis, 1901). Mathematically, the chemical potential for an ideal gas can be defined as:

$$\mu_i - \mu_i^o = RTln\left[\frac{P}{P^o}\right] \qquad (5)$$

Where μ_i is the chemical potential of component *i* in the ideal gas mixture. Since energies do not have absolute values, the subscript "*o*" is used as a reference for the partial molar Gibbs energy. When selecting a reference state, properties for that state must be specified and defined. In this case, the reference chemical potential, μ_i^o, is the chemical potential at the reference pressure P_o and at the same temperature as the chemical potential of interest, T.

Lewis, when analyzing Eq. 5 to extend it to the study of any substance that undergoes an isothermal process, introduces a pressure correction for the ideal gas state, adapting it to real substances where intermolecular interactions exist. This correction is what defines a new thermodynamic property, the fugacity, $\widehat{f_i}$, and is also known as "adjusted pressure". Eq. 6 reformulated in terms of fugitivity can be expressed as follows:

$$\mu_i - \mu_i^o = RTln\left[\frac{\widehat{f_i}}{\widehat{f_i^o}}\right] \qquad (6)$$

Therefore, in practice the chemical equilibrium criterion can be defined:

$$\widehat{f_i^{\alpha}} = \widehat{f_i^{\beta}} \qquad (7)$$

3.2 Phase Behavior

Phase behavior involves the study and characterization of the equilibrium and dynamic states of different phases in a multi-component system. The behavior of individual molecules provides the best explanation about how hydrocarbons respond to changes in pressure and temperature. The physical behavior of these molecules is influenced by three critical factors: pressure, which reflects the quantity and motion of molecules; temperature, which reflects the kinetic energy; and molecular attraction and repulsion (McCain, 2017).

3.2.1 Phase diagram for a pure substance

A phase diagram for a pure substance graphically represents the pressure and temperature conditions under which its solid, liquid, and gaseous phases coexist in thermodynamic equilibrium (Sandler, 2017). These regions are demarcated by coexistence curves**,** each corresponding to the equilibrium between two phases:

- The fusion curve separates the solid-liquid regions,
- The vaporization curve divides the liquid and gas phases,
- The sublimation curve delineates the solid and gas phases.

3.2.2 Phase diagram for binary mixtures

Understanding the fluid-phase behavior of binary systems is important in chemical thermodynamics and chemical engineering processes. Despite industrial processes involving blends of numerous compounds, binary systems remain a focal point for research, offering a means to approximate and model the phase behaviors of real mixtures. Binary systems also play a crucial role in developing complex models for mixtures, such as activity coefficient models or equations of state, where intermolecular interactions are typically assumed to be binary interactions (Privat; Jaubert, 2013).

The phase behavior of the mixtures can be represented in a diagram of pressure against composition or temperature against composition, as demonstrated in Figures 2a and 2b, respectively.

Figure 2 - (a) Vapor pressures at T = 308.15 K; and (b) boiling temperature P = 101.3 KPa, for (x_1 or y_1) c-$C_6H_{11}CH_3$+(x_2 or y_2) c-C_6H_{12}.

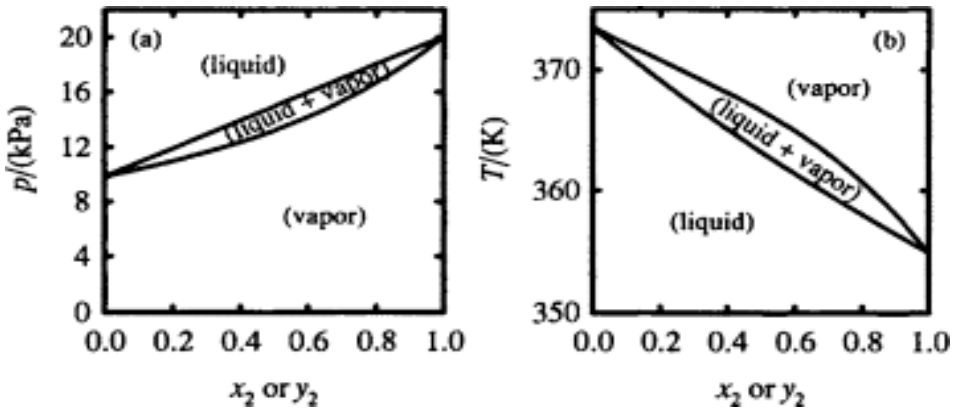

Source: Chemical Thermodynamics: Advanced Applications (2000, p. 151-159).

In Figure 2a, the upper curve shows conditions for only liquid presence, while the lower curve indicates conditions for only vapor presence. The region between them allows for the coexistence of liquid and vapor. A horizontal line, called a tie-line, drawn within this region at a constant pressure reveals the compositions of the two phases in equilibrium at that pressure.

In Figure 2b, a temperature graph is shown against composition at a fixed pressure. Only vapor is present above the upper curve, and only liquid is present below the lower curve. These diagrams are represented as a function of the composition of the most volatile component (Ott; Boerio-Goates, 2000). This system only shows liquid-vapor equilibrium (ELV).

Figure 3 illustrates a simple scenario where the bubble and dew curves consistently increase between the pure-component representative points (x_2 = 0 and x_2= 1). This behavior is expected in systems of two molecules (A and B) when the average energy of A-B interactions is similar to that of A-A and B-B interactions in the pure compounds (Privat; Jaubert, 2013).

There is also the representation of pressure-composition (P-xy) phase diagrams. For example, when the temperature equals the lowest critical temperature of a pure component, a critical point for that component emerges on the isothermal P-xy phase diagram. Subsequently, the mixture's critical point becomes a shared peak of both the bubble and dew curves, with the phase diagram remaining connected to the saturation point of pure component (2) at x_1 = 0 (see Figure 3a). This distinctive diagram is occasionally referred to as a 'racket' due to its unique shape (Privat; Jaubert, 2013).

Figure 3 - Representation of isothermal racket phase diagrams and illustration of retrograde vaporization and condensation phenomena. (a) Pure-component 1 is supercritical ($T > Tc,_1$), whereas pure-component 2 is subcritical ($T < Tc,_2$). (b) pure-component 2 is supercritical, whereas pure-component 1 is subcritical. VLE: vapor-liquid equilibrium domain, V: single vapor phase domain, L: single liquid phase domain, C: Mixture critical point.

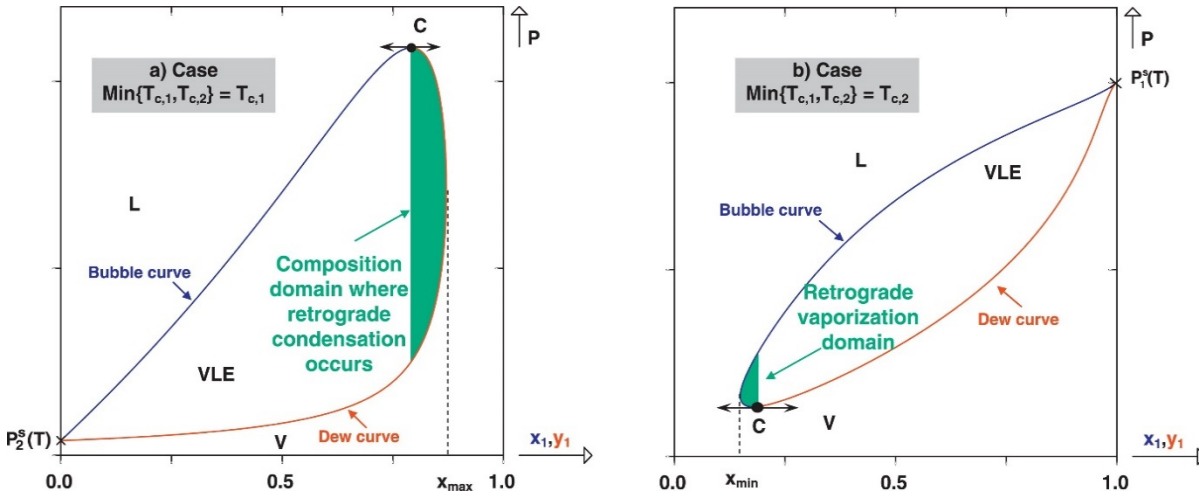

Source: (Privat; Jaubert, 2013).

In Figure 3a, during the compression of the gas initially at low pressure, retrograde condensation occurs. This phenomenon is characterized by the liquid level increasing, reaching a maximum, and then decreasing and disappearing. This happens when the critical temperature of component 1 is lower than that of component 2.

If pure component 2 becomes critical before pure component 1, the isothermal phase diagram connects to the saturation point of pure component 1 (at $x_1 = 1$). In this scenario, the mixture's critical point appears near $x_1 = 0$ and is found as a common minimum of the bubble and dew curves, as illustrated in Figure 3b. In this region, during the isothermal depletion of a liquid phase, the amount of vapor initially increases and then decreases. This phenomenon is symmetric to retrograde condensation and is called retrograde vaporization.

3.2.2.1 Classification of phase equilibrium by Van Konynenburg and Scott

For organic mixtures, Van Konynenburg and Scott (1980) have categorized phase equilibrium and critical locus typologies based on the configuration and quantity of critical lines shown on pressure-temperature diagrams.

Each of the classifications proposed by van Konynenburg and Scott (1980) is defined in the following sections. Depending on the pressure and temperature conditions,

critical lines delineate the transitions between vapor-liquid, vapor-liquid-liquid, and liquid-liquid phases. Points C_1 and C_2 represent the critical points of the more volatile and less volatile components.

Additionally, using the van der Waals equation of state as a foundation, Scott and van Konynenburg mapped out various phase behavior patterns in a parameter space diagram, thus introducing the concept of global phase diagrams. Since their initial work, significant progress has been made in understanding complex phase behavior, with further advancements derived from more sophisticated theoretical models (Polishuk; Wisniak; Segura, 2001; Schneider; Scheidgen; Klante, 2000).

3.2.2.1.1 Type I

The Type I diagram is the simplest, characterized by mixtures of hydrocarbons with similar sizes and critical properties. This results in only one ELV critical line and no liquid-liquid immiscibility between the two pure components, as shown in Figure 4.

Figure 4 - Phase diagram, Type I.

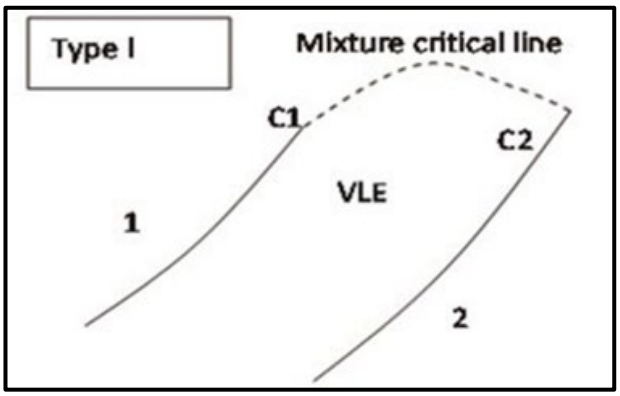

Source: Scott and van Konynenburg classification adopted by (Coquelet *et al.*, 2019).

Mixtures of substances belonging to a homologous series tend to exhibit simple phase behavior (type I) when the differences in their molecular sizes and critical properties (such as critical temperature and pressure) are small. However, if these differences in size and critical properties exceed a certain threshold, the phase behavior deviates from type I and can become more complex (Van Pelt Arnold Francis, 1992).

For studies conducted with n-alkanes and CO_2, the following examples are presented: with methane as one component, a transition from type I to type V behavior first

occurs with n-hexane (Davenport; Rowlinson, 1963), whereas, with ethane as the lighter component, n-octane is the first to exhibit partial miscibility in the liquid state (Specovius *et al.*, 1981). With propane, this behavior is observed when the second component is n-C_{30} (Peters *et al.*, 1989).

3.2.2.1.2 Type II

The type II phase diagram is characterized by immiscibility at temperatures below the critical temperature of the more volatile component, forming a second liquid phase. These mixtures exhibit a three-phase line VLLE in the *P*, *T* projection terminating at an upper critical end point (UCEP). From this UCEP, a second liquid-liquid critical curve extends to infinite pressures, as represented in Figure 5.

Figure 5 - Phase diagram, Type II.

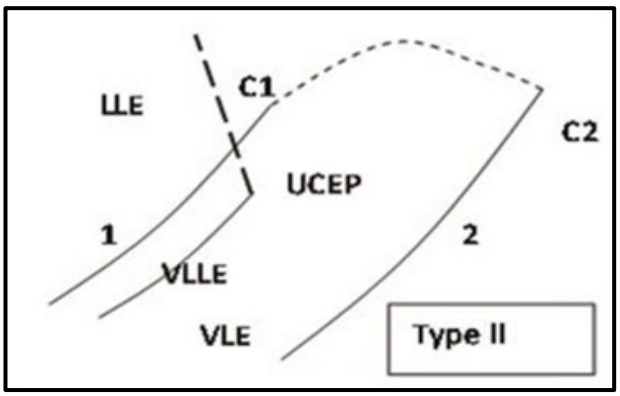

Source: Scott and van Konynenburg classification adopted by (Coquelet *et al.*, 2019).

Generally, the liquid-liquid critical curve can take one of three forms in the p, T plane, as depicted in Figure 6. These forms are described as follows:

- Curve *a*: the liquid-liquid critical curve has a negative slope in the *P,T* projection, $(\partial p/\partial T)_c < 0$.
- Curve b: the liquid-liquid critical curve has a positive slope in the *P,T* projection, $(\partial p/\partial T)_c > 0$.
- Curve c: the critical curve in the UCEP has a negative slope. At a temperature minimum, it changes to a liquid-liquid critical curve with a positive slope at higher pressures.

Figure 6 - Three possible types of critical curves in Type II mixtures.

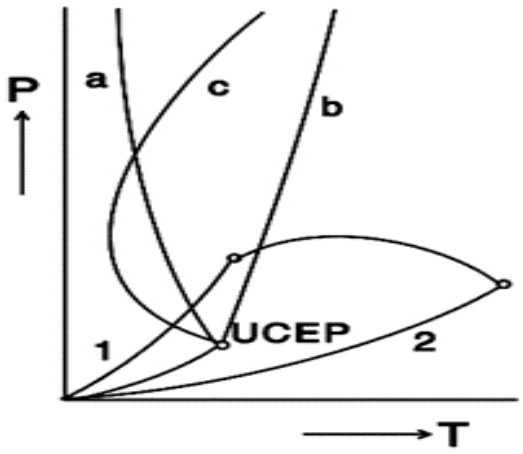

Source: (Van Pelt Arnold Francis, 1992).

Carbon dioxide + n-octane is an example of a type II system (Van Pelt Arnold Francis, 1992). Mixtures of CO_2 + n-paraffins reported by Hottovy, Luks and Kohn (1981) exhibit an VLLE region delimited by an upper critical end point (UCEP) under low-temperature conditions.

3.2.2.1.3 Type III

The third type of diagram is found in various studies involving model petroleum systems. These systems exhibit low miscibility between components, and the critical point of the less volatile component, which aligns with the VLE critical line, does not remain constant, causing a displacement of the line in the liquid-liquid-vapor region at temperatures slightly above the critical temperature of the more volatile component. The following Figure 7 illustrates the Type III diagram.

Figure 7 - Phase diagram, Type III.

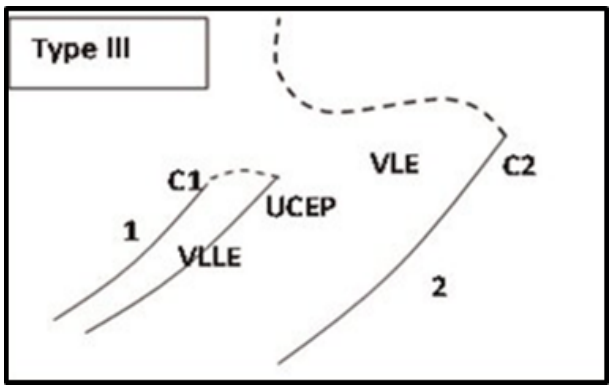

Source: Scott and van Konynenburg classification adopted by (Coquelet *et al.*, 2019).

Type III mixtures exhibit two distinct critical curves. One curve starts at the critical point of the component with the highest critical temperature and extends to infinite pressures. The other critical curve begins at the critical point of the component with the lowest critical temperature and intersects a three-phase line VLL at an UCEP (Van Pelt Arnold Francis, 1992).

3.2.2.1.4 Type IV

The phase behavior characteristics of mixtures represented by Type IV diagrams exhibit three critical lines, as shown in Figure 8.

Figure 8 - Phase diagram, Type IV.

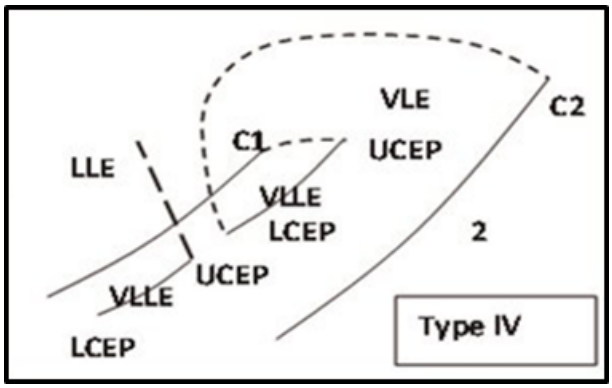

Source: Scott and van Konynenburg classification adopted by (Coquelet *et al.*, 2019).

The first line extends from the liquid-liquid equilibrium (LLE) region to the UCEP at low pressure and temperature conditions. The second line, which delineates the VLE region,

extends from point C_2 to the lower critical end point (LCEP) of a vapor-liquid-liquid equilibrium (VLLE) region, where the temperature is lower than the critical point C_1. Finally, the third line extends from point C_1 to another point, also termed UCEP, which represents the boundary of another VLL region of the mixture (Medeiros *et al.*, 2023). It is known that Type IV phase behavior occurs in the binary systems methane + 1-hexene (Davenport; Rowlinson; Saville, 1966) and CO_2 + n-tridecane (Van Der Steen; De Loos; De Swaan Arons, 1989).

3.2.2.1.5 Type V

Type V mixtures feature two distinct critical curves, similar to Type IV, but without a pronounced liquid-liquid critical curve. Figure 9 represents the Type V phase diagram.

Figure 9 - Phase diagram, Type V.

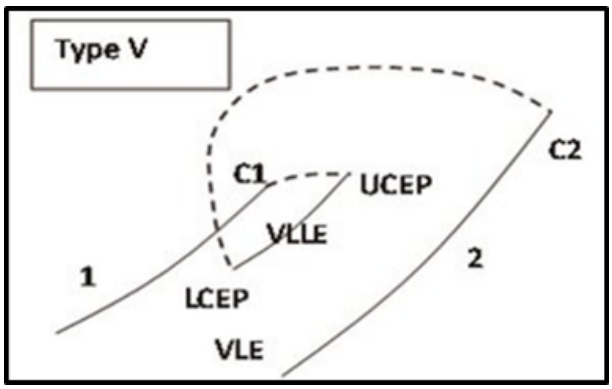

Source: Scott and van Konynenburg classification adopted by (Coquelet *et al.*, 2019).

However, in mixtures known as Type V, the distinguishing liquid-liquid critical curve may be obscured by forming a solid phase (Van Pelt Arnold Francis, 1992). In addition, the UCEP and LCEP points bound the immiscibility region, respectively, showing that there are no two liquid phases for pressure and temperature values below the LCEP.

An example of a mixture exhibiting Type V behavior is the methane + n-hexane system (Davenport; Rowlinson, 1963). In this system, immiscibility is observed: at temperatures below the LCEP (182.46 K) (Chen Roger J. J.; Chappelear Patsy S.; Kobayashi Riki, 1976; Lin; Hwang; Kobayashi, 1978), methane and n-hexane are fully miscible in the liquid state.

3.2.2.1.6 Type VI

Type VI diagrams show two critical lines. The first is a continuous vapor-liquid critical curve that connects the critical points of the pure components. The second critical curve is defined within a specific range of temperature and pressure, where a VLLE is observed. These diagrams present a closed liquid-liquid critical curve that begins at a LCEP on a three-phase line VLLE and ends at a UCEP on the same three-phase line, caused by the tilt of both critical lines. The following Figure 10 shows the Type VI phase diagram.

Figure 10 - Phase diagram, Type VI.

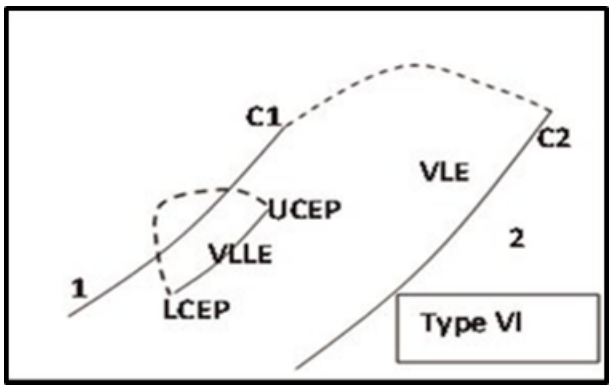

Source: Scott and van Konynenburg classification adopted by (Coquelet *et al.*, 2019).

Type VI phase behavior is found in mixtures where strong intermolecular bonds, such as hydrogen bonds, can form.

3.2.2.2 Algorithm to define the type of phase diagram in a binary mixture

Cismondi and Michelsen (2007) developed an algorithm to identify the three ways the critical line, starting from C_2 (the critical point for the pure component with the highest critical temperature), extends to different endpoints. This is illustrated in Figure 11.

Figure 11 - Algorithm to identify the three ways the critical line extends to different endpoints, starting from C_2 (the critical point for the pure component with the highest critical temperature).

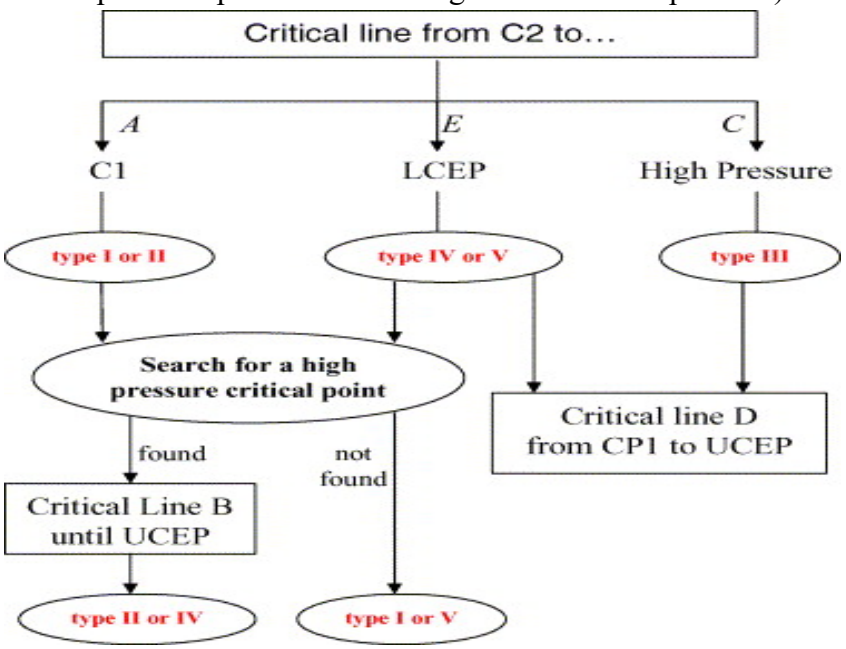

Source: (Cismondi; Michelsen, 2007)

3.2.3 Phase behavior of ternary mixtures

This diagram generally assumes a constant pressure, often atmospheric pressure, while representing temperature and two concentration parameters as variables. It is important to note that one degree of freedom is used when setting the pressure, which simplifies the diagram but must be taken into account when applying the phase rule in analyses. This approach helps to understand how different phases coexist in the system under different conditions (Campbell, Flake C., 2012).To fully describe the phase equilibria at constant pressure in a ternary system, it is necessary to use a three-dimensional diagram. This approach assigns two dimensions to represent composition and a third dimension for temperature.

Since the pioneering work of van Konynenburg and Scott (1981) on the global phase behavior of binary mixtures, research has been conducted to classify the types of global phase behavior in ternary systems. However, no equivalent classification scheme has been established for ternary mixtures.

Phase diagrams and critical states of ternary mixtures can be obtained using the van der Waals equation of state with standard mixing rules based on the single fluid model. For binary interaction parameters, Berthelot-Lorentz (Mainwaring; Sadus; Young, 1988) combination rules apply. The different topological classifications of the generated ternary phase

diagrams are identified and how they relate to the corresponding classes of their binary subsystems is analyzed. Furthermore, it is shown that phenomena such as miscibility windows and miscibility islands are associated with a specific class of ternary phase diagram and can even be modeled using the van der Waals equation of state (Bluma; Deiters, 1999).

3.2.3.1 Classification of Ternary Phase Diagrams

Through the combined application of the Berthelot-Lorentz rules, eight primary classes of phase diagrams for ternary systems have been identified. These classes, along with their corresponding binary subsystems, are summarized in Table 1.

Table 1 - Phase diagrams classes for ternary systems and their corresponding binary subsystems.

Binary subsystems			**Ternary class**
I	I	I	T-I
I	I	II	T-II
I	I	III	T-III
I	II	II	-
I	II	III	T-V
I	III	III	T-IV, T-V
II	II	II	T-VIII
II	II	III	-
II	III	III	-
III	III	III	T-VII

Source: (Bluma; Deiters, 1999).

Ternary Class I: Phase diagrams in this class feature closed *lg* (liquid-gas)-critical curves connecting the three critical points of the pure components. All binary subsystems belong to Type I (as per van Konynenburg and Scott, 1981), and this class is exclusive to chemically similar compounds.

Ternary Class II: This ternary phase diagram includes two Type I and one Type II binary subsystems. As a result, in addition to the lg-critical surface, a *ll* (liquid-liquid)-critical plane appears at low temperatures. Under low-pressure conditions, this plane is delimited by a curve of critical endpoints, which indicates the beginning of a three-phase region. This curve, composed of upper critical endpoints, is called the upper critical line (UCEL).

Ternary Class III: This diagram presents two Type I and one type III binary subsystems. It includes a single continuous critical plane. The UCEL line ends at a tricritical point, while, on the opposite side of the discontinuity, the critical plane extends to infinite pressures. In this region, a gradual transition occurs between *lg* and *ll* phase equilibria.

Ternary Class IV: This class occurs when one of the binary subsystems is Type I, while the other two are Type III. A typical example includes systems composed of two similar heavy components and one very light component that exhibits Type III behavior with each of the heavy components. In this case, a broad critical surface is observed extending toward high temperatures and infinite pressures, along with a smaller critical surface at low temperatures, bounded by a UCEL line.

Ternary Class V: In this class, the binary subsystems correspond to Types I, II and III. Its behavior is very similar to that of class III, but with the difference that an additional ll-critical surface appears in the low temperature region.

Ternary Class VI: This class is the contrast to the ternary class IV. As in that class, the binary subsystems are type I, III and III, but in this case, it is a mixture of two similar light compounds with one heavy one. There are two critical surfaces, the lower one being delimited by a UCEL.

Ternary Class VII: All binary subsystems in ternary class VII are of binary Type III. This ternary phase diagram presents three critical planes: one for the component with the highest critical data, showing ll-critical behavior, another for the component with the lowest critical data, showing lg-critical behavior, and a third component with a critical plane that combines ll-critical and lg-critical behavior.

Ternary Class VIII: Finally, there is a ternary class in which all binary subsystems are Type II. This phase diagram presents a continuous lg-critical surface, similar to class I, along with three ll-critical surfaces at low temperatures. Depending on temperature ranges and binary interaction parameters, several subtypes may exist, although in practice the ll surfaces are usually obscured by crystallization.

If more variations in the molecules and their interactions are allowed, the number of possible types of ternary phase diagrams increases significantly. However, in practice, this number is reduced because liquid-liquid immiscibility is often masked by crystallization (Bluma; Deiters, 1999).

Another study conducted by Francis (Francis, Alfred W., 1954) examined 464 ternary phase diagrams involving carbon dioxide at or near ambient temperature, using a solvent compound and a hydrocarbon. The study revealed a wide variety of phase behaviors.

3.3 Thermodynamic Properties

3.3.1 The Critical Point

Figure 12 shows a PV phase diagram where each line represents an isotherm, illustrating how volume increases as pressure decreases. At the two lowest temperatures, the isotherms begin in the liquid phase. As pressure decreases, the saturation pressure point is reached. In the two-phase region, pressure remains constant because P and T are no longer independent variables. At higher temperatures, the saturated liquid volumes increase, while the saturated vapor volumes decrease. The critical point is defined at the top of the liquid-vapor phase envelope, where the values of V_l and V_v become identical. This point is characterized by the critical temperature, *Tc*, and critical pressure, *Pc*. Beyond this point, the distinction between the liquid and vapor phases ceases to exist, rendering the region indistinguishable as either phase.

Figure 12 - PV diagram. Four isotherms are shown: - two below the critical temperature (subcritical), one at the critical temperature, and one above the critical temperature (supercritical).

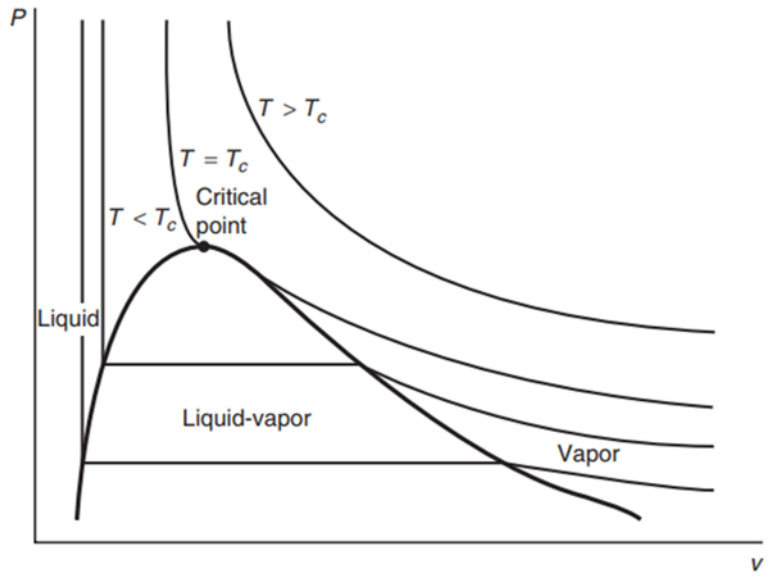

Source: Engineering and Chemical Thermodynamics (2012, p.43).

3.3.2 Saturation Pressure

Saturation pressure is defined as the pressure at which a given substance boils at a specific temperature. This concept differs significantly from vapor pressure, which refers to the

contribution of a substance to the total pressure in a mixture at a given temperature. This contribution corresponds to the partial pressure of the substance in an ideal gas mixture.

Figure 13 provides a schematic representation of these definitions. On the left side, two piston-cylinder systems illustrate the saturation pressure at different temperatures. In each system, there is only one pressure at which the two phases can coexist in equilibrium, defined as the saturation pressure, P^{sat}. On the right side, the vapor pressure for the two systems is depicted. To determine the vapor pressure of species a, it is necessary to calculate its contribution to the total pressure of the mixture.

Figure 13 - Graphical representation of the saturation pressure of pure *a* and the vapor pressure of *a* and *b*. Two temperatures, T_1 and T_2 are shown.

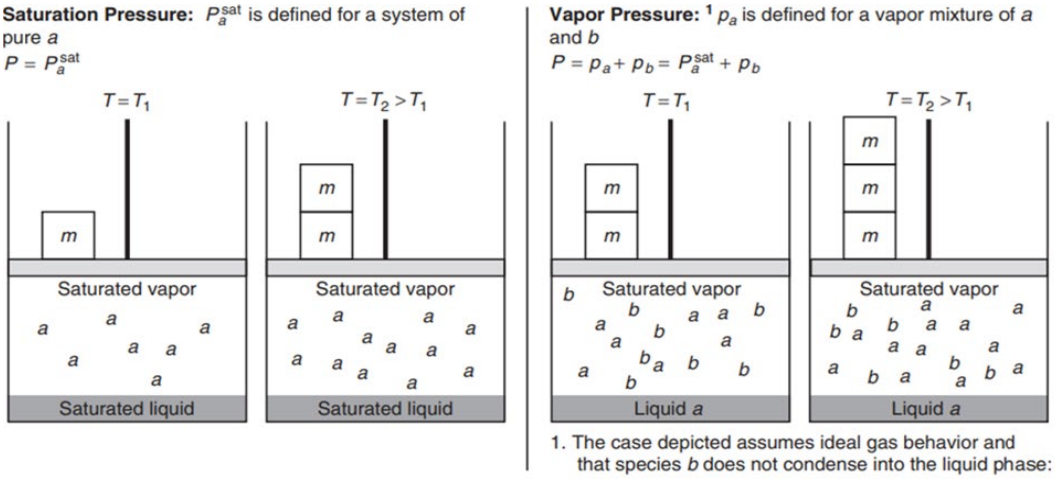

Source: Engineering and Chemical Thermodynamics (2012, p.41).

3.4 Cubic Equation of States (Cubic EoS)

The objective of the equations of state originated due to the interest in arriving at an equation that relates the measured variables P, V and T through the adjustment of experimental data.

The ideal gas equation is an empirical model derived from experimental observations (Boyle's, Charles's, and Avogadro's laws). It serves as a limiting case for gases at low pressures and high temperatures, where intermolecular forces and molecular volume are negligible. The van der Waals equation, proposed in 1873, represents a significant improvement over the ideal gas model by incorporating corrections for molecular volume and intermolecular forces (Koretsky, 2013). This adjustment yields the following equation, Eq. 8:

$$PV^3 - (RT + Pb)V^2 + aV - ab = 0 \qquad (8)$$

where *a* and *b* are defined as the repulsive parameter and the co-volume, respectively.

To apply the van der Waals equation, it is necessary to determine the parameters a and b specific to the substance in question. The most accurate values are obtained by fitting experimental data of PVT. However, in the absence of such data, the principle of corresponding states can be used as an alternative.

The principle of corresponding states allows the properties of a substance to be scaled based on their values at the critical point. The van der Waals parameters can be linked to the critical temperature and pressure by considering that the critical isotherm presents an inflection point. This can be expressed mathematically as follows:

$$\left(\frac{\partial P}{\partial V}\right)_{T_c} = \left(\frac{\partial^2 P}{\partial V^2}\right)_{T_c} = 0 \qquad (9)$$

Thus, at the critical point the following values are obtained:

$$a = \frac{27}{64}\frac{(RT_c)^2}{P_c} \qquad (10)$$

$$b = \frac{(RT_c)}{8P_c} \qquad (11)$$

where, *Tc* and *Pc* are the temperature and pressure of the compound at the critical point.

The Peng-Robinson (PR) equation of state, introduced in 1976 (Peng; Robinson, 1976), represents a pivotal advancement in thermodynamic modeling of fluids, particularly for systems involving hydrocarbons and asymmetric mixtures. Its formulation addresses critical limitations of earlier cubic equations, such as the van der Waals equation, by refining the mathematical description of intermolecular attraction and repulsion. The generalized form of the PR equation is expressed as:

$$P = \frac{RT}{V_m - b} - \frac{a}{(V_m + b)(V_m - b)} \qquad (12)$$

Where V_m is the molar volume, P is pressure, T is temperature, and R is the universal gas constant.

3.5 Experimental Methods for Fluid Phase Equilibria

Various techniques are utilized to study the phase behavior of multicomponent mixtures under high-pressure and high-temperature conditions. The reviewed studies fall into two categories of methods. The classification of these techniques is based on how composition is determined. In the analytical method, compositions of coexisting bulk phases are determined through sampling and chromatographic analysis. In contrast, the synthetic method experimentally determines the overall composition by metering the amounts of each pure substance introduced into the apparatus (Al Ghafri, Saif, 2013).

3.5.1 Analytical Method

In the analytical method, the overall composition of the mixture is often not known at the beginning of the experiment. The compositions of the coexisting phases at equilibrium can be determined through two main approaches: (1) in situ analysis, where the spectrophotometer is directly connected to the equilibrium cell (EC), allowing real-time measurement without the need for sampling, or (2) by extracting samples from the system at various stages for subsequent analysis of their compositions. This latter approach involves taking samples from the system and analyzing them later to determine the phase compositions (Balbinot Filho *et al.*, 2023). To avoid pressure drops during large sampling, variable-volume cells or buffer autoclaves are employed, ensuring minimal impact on phase composition.

3.5.2 Synthetic Method

Synthetic methods involve preparing a mixture with a known composition and observing its phase behavior in an equilibrium cell while measuring properties such as pressure and temperature. This approach eliminates the need for sampling and instead focuses on directly preparing and analyzing the mixtures.

By controlling the composition of the mixture from the outset, the method simplifies the analysis process compared to traditional techniques that require sampling and analysis of unknown mixtures. It can be applied with or without a phase transition, requiring the preparation of a mixture with a precisely known composition in both cases.

In synthetic methods with a phase transition, temperature and pressure are adjusted to achieve homogeneity, and then they are varied until the formation of a second phase is observed. The composition of the first phase is set to the known overall composition, while the composition of the second phase remains unknown. Each experiment provides one point on the PTx phase envelope (Fonseca; Dohrn; Peper, 2011).

These methods are categorized into visual and non-visual approaches. Visual methods rely on direct observation of a new phase, applicable to various equilibria and critical curve determination. Non-visual methods detect phase transitions by monitoring alternative physical properties. Examples include X-ray transmission, microwave technology, and spectroscopy techniques for in-situ observation. These methods enable the determination of dew and bubble points and have been successfully applied to various fluid mixtures in multiple studies conducted by researchers (Dohrn; Peper; Fonseca, 2010).

3.5.2.1 Visual Synthetic Method

In the visual synthetic method, phase detection is primarily achieved through direct visual observation. This technique relies on indicators such as turbidity or meniscus formation within a view cell to identify the appearance of new phases. The method is notably versatile, extending its applicability beyond the determination of vapor-liquid equilibria to encompass a wide range of complex phase behaviors. It is effectively used to study multiphase equilibria, liquid-liquid separations, solid-liquid equilibria, liquid-liquid-vapor equilibria, critical curves of mixtures, gas hydrate formation, cloud-point determination, and phase equilibria in polymer-solvent systems. By utilizing these visual cues, researchers can comprehensively analyze phase transitions and equilibrium states, making this approach an invaluable tool in the study of phase behavior (Fonseca; Dohrn; Peper, 2011).

In the static synthetic method, the global composition of the mixture is measured prior to introducing it into the equilibrium cell. This cell, which features a variable volume, includes a piston driven by a hydraulic pump to regulate the pressure within the system. The experiment begins with a single-phase mixture at specified pressure and temperature conditions. As the pressure is gradually reduced, different phases begin to emerge. These phases are visually identified by observing bubbles, turbulence, or mist. The main disadvantage associated with the utilization of this apparatus is the time expended in discharging, disassembling, cleansing, assembling, and loading for each alteration in global composition (Leal, Monique Ferreira, 2015).

Static methods involve the use of cells with either constant or variable volumes, which can be categorized as constant-volume static cells (CVSCs) and variable-volume static cells (VSCs). In VSCs, the pressure within the system can be adjusted by moving a piston inside the cell, allowing for precise control over the experimental conditions. These conditions of pressure, temperature and composition in equilibrium are reported resulting in a PTx phase diagram, useful to describe and analyze the behavior of the mixtures at different operating conditions (Fornari; Alessi; Kikic, 1990).

3.6 Experimental data founded in the literature

This section will be dedicated to compiling research on binary systems composed of the substances used in the model systems that are part of this study's objective. It is important to note that there are no previous studies on these ternary systems in the literature. Therefore, the primary focus is on a binary system composed of CO_2 + n-$C_{16}H_{34}$ and CO_2 + n-$C_{10}H_{22}$.

A literature review searching for data availability for carbon dioxide (CO_2) + decane (and/or + hexadecane) and mixtures with oil or synthetic oil that could closely resemble the behavior of petroleum fluid was done, as summarized in Table 2. This work investigated a ternary system (decane + hexadecane + carbon dioxide) at pressure conditions up to 30 MPa. Moreover, it focused on a composition range from 20% to 98.5% mol CO_2, where regions of LLE and VLLE were observed at high CO_2 compositions at the temperatures of 283.15 K and 298.15 K. The pressure and temperature operational conditions are very similar to those reported in Table 2.

Table 2 - Summary of published data for systems containing CO_2 with decane, hexadecane, and oil or synthetic oil.

System	Type of Data	Pressure Range (MPa)	Temperature Range (K)	Source
CO_2 + decane	VLE	0-18.84	255.4-510.9	(Reamer; Sage, 1963)
	LLVE	0.10-1.64	217.2-248.7	(Kukarni *et al.*, 1974)
	VLE	1.96-5.12	462.6-583.6	(Sebastian *et al.*, 1980)
	VLE	6.38-16.4	344.3-377.6	(Nagarajan; Robinson, 1986)
	VLE	5.15-14.24	342.9-594.2	(Inomata *et al.*, 1986)
	VLE	4.7-15.5	344.2-377.5	(Chou; Forbert; Prausnitz, 1990)
	VLE	0.89-12.70	344.3	(Shaver; Robinson; Gasem, 2001)
	VLE	2.58-11.59	344.3-344.8	(Tsuji *et al.*, 2004)
	VLE	3.48-16	319.1-372.9	(Jiménez-Gallegos; Galicia-

				Luna; Elizalde-Solis, 2006)
	VLE	1.73-10.11	344.25	(Ren; Scurto, 2007)
	VLE	5-14	308-348	(Zamudio; Schwarz; Knoetze, 2011)
	VLE	2-20	304-618	(Juntarachat *et al.*, 2012)
	VLE	3.25-10.80	308.15-343.15	(Yang *et al.*, 2012)
	VLE	1-6	323.2	(Kariznovi; Nourozieh; Abedi, 2013)
	VLE	0-14	311 and 344.3	(Forte; Galindo; Trusler, 2011)
	VLE	1.7-12.7	319-355	(Fele Žilnik *et al.*, 2016)
	VLE	3.4-76.4	313-410	(Kandil; Al-Saifi; Sultan, 2016) (Nascimento *et al.*, 2019)
	VLE	2.42-7.29	313.2-353.2	
CO_2 + hexadecane	LLVE	1.57-14.80	280.25-367.5	(Schneider *et al.*, 1967)
	VLE	2.01-5.09	436.4-664.1	(Sebastian *et al.*, 1980)
	LLVE	0.69-25.9	308.2-343.2	(Charoensombut-amon; Martin; Kobayashi, 1986)
	VLE	7.69-16.12	314.2-353.2	(D'souza; Patrick; Teja, 1988)
	VLE	10.0-25.1	333.2-393.2	(Hölscher; Spee; Schneider, 1989)
	LLVE	4.40-7.48	283.2-306.1	(Van Der Steen; De Loos; De Swaan Arons, 1989)
	VLE	10.1-25.6	294.4-413.3	(Spee; Schneider, 1991)
	VLE	1.24-3.29	305.7-512.3	(Breman B. B. *et al.*, 1994)
	VLE	10.1-25.7	473.2-573.2	(Brunner; Teich; Dohrn, 1994)
	VLE	10.0-20.0	353.2	(Kordikowski; Schneider, 1993)
	VLE	2-35	313.15, 353.15 and 373.15	(Venter *et al.*, 2007)
	VLE	0.1-23	308-358	(Latsky; Cordeiro; Schwarz, 2020)
	LLVE	0.1-58	293.1-353.1	(Simoncelli *et al.*, 2020)
Crude oil and synthetic crude oil	LLVE	0.10-7.52	305.2-322.2	(Orr; Jensen, 1984)
	LLVE	0-20	305.2	(Nghiem; Li, 1986)
	LLVE	5.50-11.03	304.3-307.6	(Creek; Sheffield, 1993)
	LLVE	36-40	298.15-473.15	(Al Ghafri; Maitland; Trusler, 2014)
	VLE	0-12	323.15	(Han *et al.*, 2015)
	LLVE	3-30	293.15-353.15	(Lucas *et al.*, 2016)
	VLE	35-40	293.15, 323.15 and 373.15	(Elias; Trevisan, 2016)
	LLVE	0-100	293.15-378.15	(Romero Yanes *et al.*, 2020)
	VLE	3.63-72.48	313.15-393.15	(Medeiros *et al.*, 2023)

Source: Created by the author.

3.7 Barotropic inversion

When temperature or pressure changes, both the compositions and properties of the coexisting phases, such as density and refractive index, often change. In some cases, the difference in density between the phases can decrease and even reverse their values, a behavior known as “barotropy”. The point where this inversion occurs is called the “isopycnic point”.

Also known as density inversion, phase inversion and barotropic phenomenon, according to the study by Quinteros-Lama et al. (Quinteros-Lama *et al.*, 2015), these density inversions can be observed within practical temperature ranges, where a change occurs in the size of the most dense and compact part of the component molecules. The study also concludes with the possibility of observing density inversions in immiscible liquid phases or between a liquid and a gas phase.

Additionally, barotropy is often observed in systems composed of an organic compound with relatively low liquid density (such as hydrocarbons or alkanols) and a supercritical solvent with high critical density (like carbon dioxide, sulfur hexafluoride, certain fluorocarbons, or xenon). In such systems, barotropy is more common than not and can play a significant role in separation processes where phase stratification is crucial, such as in supercritical fluid extraction (SFE) (Schneider; Scheidgen; Klante, 2000).

According to the conclusion of the work conducted by Quiñones-Cisneros (Quiñones-Cisneros, 2004), the emergence of the barotropic phenomenon is suggested as an alternative for the transition between Type II and Type III phase behavior. Using the PC-SAFT EOS, this work modeled and developed figures showing the molar isopycnic curve near the critical point of pure CO_2.

In the case of barotropic behavior induced by asymmetry, one of the necessary conditions for molar density inversion to occur is that the molar mass of species h (denoting the component with the highest critical point, n-alkane), referred to as the heavier component M_{wh}, must be greater than that of the smaller molecules, the more volatile component M_{wl}.

This is the case with CO_2 + alkane mixtures (above propane). This follows the rule that molar isopycnicity implies mass isopycnicity as long as Mwh> Mwl. Once a molar density inversion occurs, the subsequent mass density inversion will depend on the actual relationships between the molar masses of the compounds.

In such cases, depending on the molecular weights of the phases involved, gravitational fields may not necessarily influence the behavior of the mixture. Consequently, unlike mass barotropic behavior, molar density inversions (MoDI) (or molar barotropic

behavior) are not directly observable in phase equilibrium experiments. Instead, they must be detected by directly measuring molar densities or using precise equations of state (EOS) to predict the molar density of the coexisting phases (Flores *et al.*, 2012).

Flores *et al.* (Flores *et al.*, 2012) concluded with the following observations: for the existence of a barotropic inversion in carbon dioxide + hydrocarbon mixtures, a mathematical framework must be in place:

I. In asymmetric mixtures like CO_2 with hydrocarbons, there is a complex point in the phase diagram called a mathematical double point (MDP). This point is where two-phase instability curves (spinodals) intersect or are very close to each other. This molar barotropic phenomenon is strongly linked to Type III phase behavior, characterized by the coexistence of three phases (liquid-liquid-vapor) and immiscibility in the liquid phases at high pressures and low temperatures. In summary, the presence of this MDP in asymmetric systems explains why this complex behavior is observed in the phase diagram.

II. In barotropic behavior caused by asymmetry, a molar density inversion must occur for a mass density inversion to take place.

III. For strong barotropic behavior, the critical curves of the pure components must be “well-separated”, meaning they should neither intersect nor merge in the phase diagram. This condition implies that each pure component must have a distinctly defined critical point, independent from the critical point of the other component. This behavior is particularly relevant in the study of asymmetric mixtures, indicating that the separation of critical curves is a necessary condition for the pronounced manifestation of barotropic phenomena in the system.

Furthermore, the conclusions drawn from the work of (Flores *et al.*, 2012) are as follows: Increased molecular asymmetry promotes mass barotropy in mixtures. In CO_2 + hydrocarbon mixtures, it has been demonstrated that mass barotropy is most likely to occur in Type III and IV systems, while Type II systems may also exhibit density inversions. Lastly, it is concluded that in Type II systems, the dominant effect is a positive synergy within the mixture rather than molecular asymmetry.

Figure 14 shows the pressure-composition phase diagrams before and after the three-phase coexistence curve. Under subcritical conditions, liquid-vapor behavior is present, and the liquid and vapor binodal curves will connect the liquid and vapor saturation molar volumes of the pure components, as seen in the 250 K phase diagram.

For asymmetric mixtures with large molar masses, the difference in the coexisting molar volumes can be substantial, and the tie-lines can have a lower slope. However, as an incipient third liquid phase develops, the three-phase triangle opens to a tie line $L_1 - L_2$ tangential to the liquid binodal curve. In other words, transitioning from an $L_1 - V$ tie line to an $L_1 - L_2$ tie line will require a rotation of around 90°(Quiñones-Cisneros, 2004).

Figure 14 - Pressure - composition phase diagrams for the CO_2 + n-C_9 mixture before and after the three phases critical end-point in a type II phase behavior system.

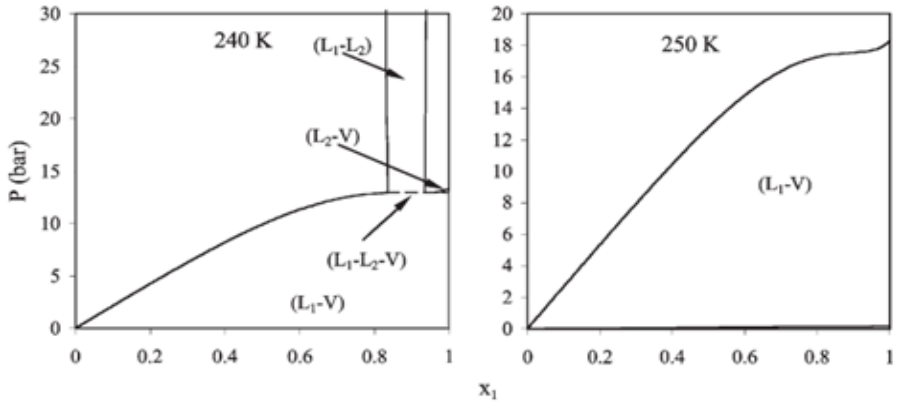

Source: (Quiñones-Cisneros, 2004).

Similarly, according to work conducted by Tardón (Tardón *et al.*, 2012), molar isopycnicity is present in phase behaviors of Types II, III, IV, and V. From this, it can be inferred that molar density inversions are more common than previously thought and that the liquid phase provides a natural condition for their existence.

In line with the previous study, this dependency is defined by differences in molecular size and critical properties. Molar isopycnicity becomes observable within ranges where stable fluid phases can be seen as the molecular size ratio of the constituents increases. Moreover, differences in critical properties promote more comprehensive temperature ranges for molar density inversions.

The literature review did not identify any recent experimental studies reporting density inversion in mixtures containing CO_2. However, there are older studies that model the behavior of binary and ternary systems and predict molar isopycnicity in these systems: ethane

+ n-alkylbenzene (Jangkamolkulchai; Arbuckle; Luks, 1988), methane + ethane + n-docosane and methane + ethane + n-tetradecylbenzene (Jangkamolkulchai; Luks, 1989), ethane + n-paraffin mixtures (Estrera, Susana S.; Luks, Kraemer D., 1987), ethane + 1-decanol + n-docosane (Hong; Patton; Luks, 1994).

Based on the evidence obtained from these experiments, it is likely that molar density inversions occur in partially miscible mixtures. These mixtures typically consist of volatile solvents - either organic or inorganic - and heavy chain solutes, and they behave as Type III or Type V systems according to the van Konynenburg and Scott (1980) classification (Charos *et al.*, 1985).

Figure 15 shows a PT projection diagram for the CO_2 + n-$C_{16}H_{34}$ system (Flores *et al.*, 2012), characteristic of a Type III diagram. The figure shows the mass isopycnicity between the fluid phases along the MaDI line A-B (mass density inversion), represented by the blue line, where a gravitational density inversion change can be experimentally observed.

Figure 15 - P–T projection for the binary system of CO_2 + $C_{16}H_{34}$ (Mw_2 = 226.45, k_{12} = 0.12). (**o**) Pure component critical point, (—o—) three-phase (or LLV) line, (· · ·) pure component vapor pressure line, (—) critical line, (—◊—) MaDI line, and (—□—) MoDI line.

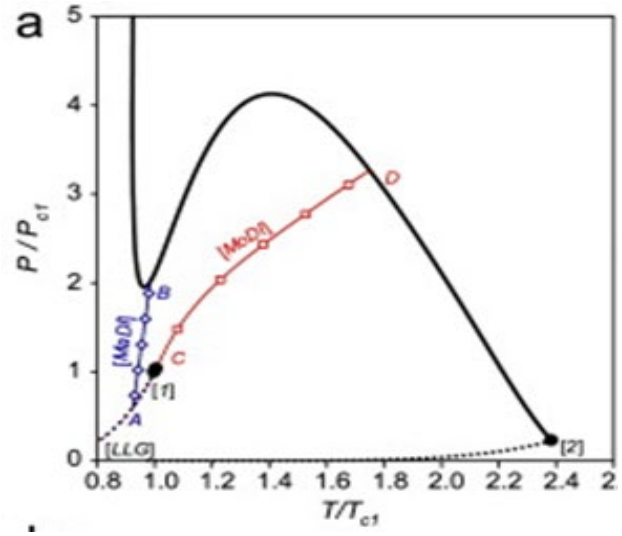

Source: (Flores *et al.*, 2012).

In detail, the MaDI and MoDI lines intersect with the mixture's critical line (indicated by points B and D). From this figure, it can be deduced that mass and molar density inversions occur between two coexisting fluid phases, which become indistinguishable as they approach the critical point. The diagram also identifies the critical mass inversion point (CMaDIP) and critical molar density inversion point (CMoDIP). The CMaDIP, shown by point B, occurs near

the critical temperature of CO_2. The CMoDIP, identified as point D, occurs at higher temperatures and pressures.

4 MATERIALS AND METHODOLOGY

4.1 Materials

Table 3 summarizes some information regarding chemicals used in this study. All the components were used without any further treatment.

Table 3 - Properties of pure compound considered in this work.

Chemical name	CAS	Source	Mole fraction purity*
Carbon dioxide	124-38-9	White-Martins	0.9999
Decane	124-18-5	Sigma-Aldrich	0.99
Hexadecane	544-76-3	Sigma-Aldrich	0.99

*Purity provided by the suppliers.
Source: Created by the author.

4.2 Experimental Methodology

Complex transitions phase behavior analysis has been carried out using a high-pressure volume variable pump, as shown in the schematic drawing in Figure 16 and the equipment design in Figure 17. The equilibrium cell, with a total internal volume of 30 mL, comprises two sapphire windows: a small lateral one that allows illumination through an optical fiber and a larger one at the front of the cell, enabling interior visualization through a high-end digital microscope.

The upper section has three ports for installing the two measurement devices (pressure and temperature transducer) and the injection valve, which allows the entry of both liquid and gas. One of the devices is the Mensor Wika pressure transducer (0-100 MPa) with an uncertainty of ±0.02 MPa, which allows the pressure monitoring of the fluid inside the PVT cell. The pressure gauge is connected to the PVT cell, presenting a minimum dead volume. Another is a temperature sensor using a Pt-100 thermocouple with an uncertainty of less than 0.1 K.

Figure 16 - Schematic diagram of the PVT cell.

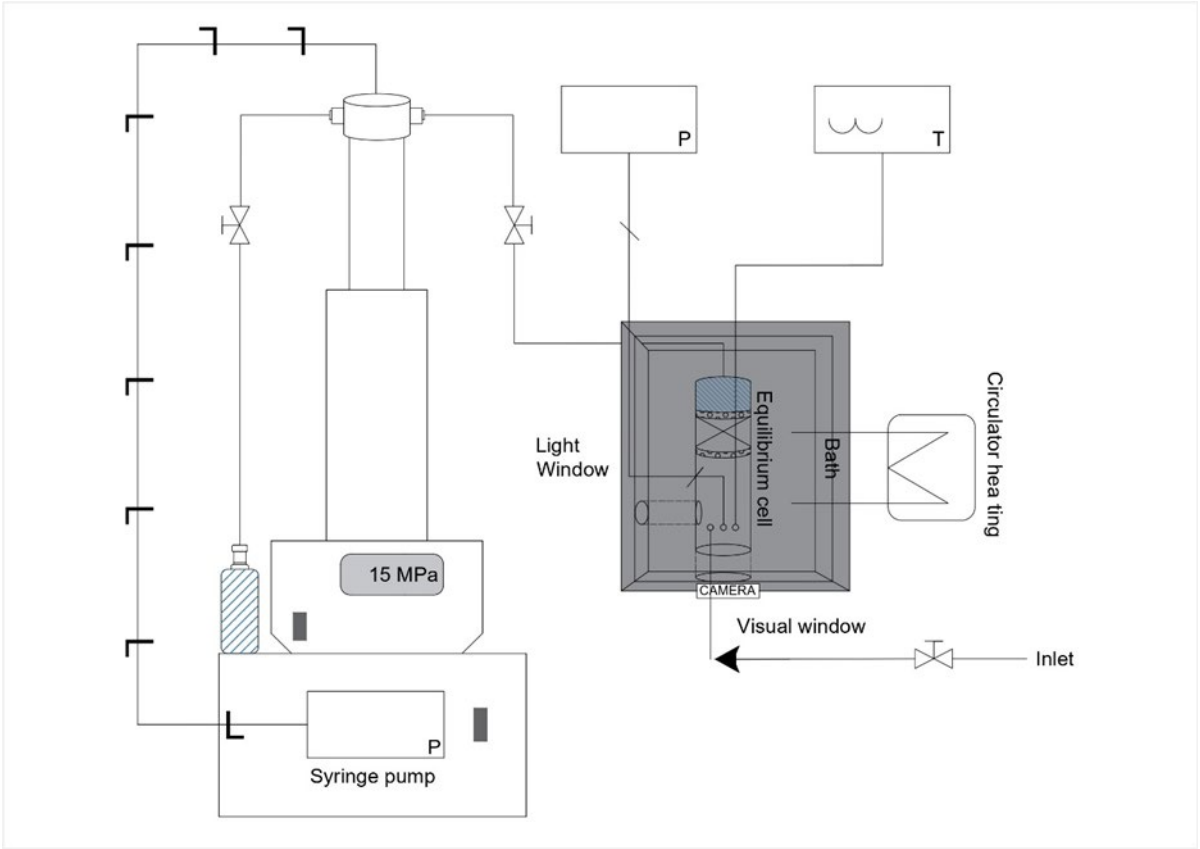

Source: Adapted from (Valero; Maria, 2020).

Figure 17 - Equipment design (Syringe pump, assembled PVT cell, thermal bath).

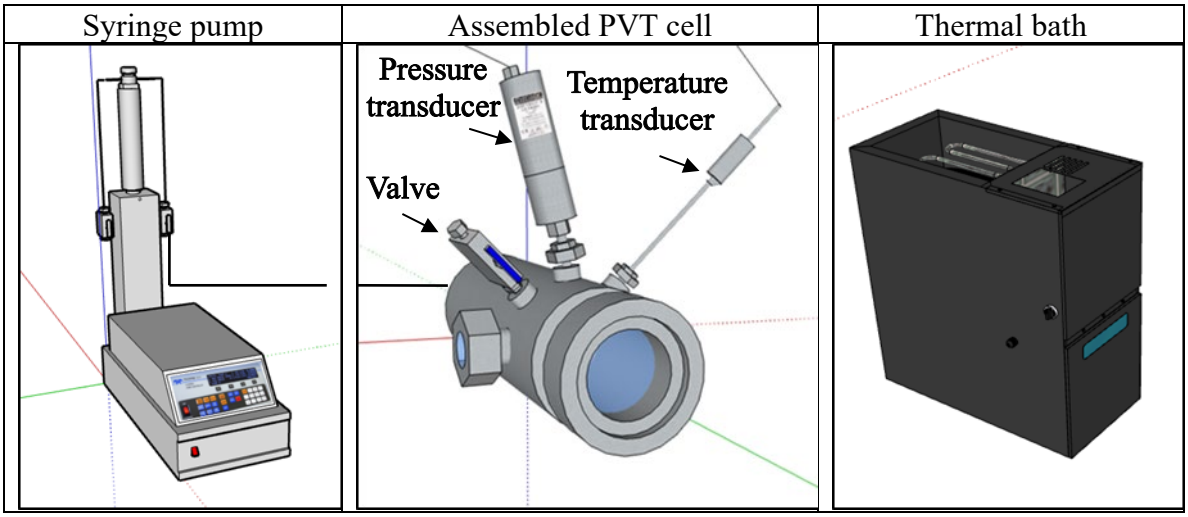

Source: Created by the author (2024).

The cell features an internal piston, one face in direct contact with the system, and the opposite side connected to a Teledyne Isco Model 260 D water pump. This setup enables

the control of sample pressure by adjusting internal volume changes. A controlled temperature oil bath generates sample heating by circulating a heat-carrier (Thermal H10) fluid. Additionally, a magnetic stirrer was put inside the cell, and the system was positioned above stirring equipment to ensure constant mixing and homogeneity of the mixture.

Before initiating any experiment, the cell is disassembled and cleaned using hexane as a solvent. After that, a validation test was conducted using nitrogen at a pressure of 8 MPa and room temperature to ensure system integrity. Binary and ternary composition systems were precisely prepared gravimetrically by weighing each component using a high-precision balance (Sartorius) with the uncertainty of 0.01 g for CO_2 and 0.005 g for the liquid mixture. The liquid mixture was first injected into the PVT cell under vacuum using a capillary tube constantly immersed in the small flask. Once the liquid is inside the cell, a known amount of CO_2 is injected to reach a desirable global mole composition. Figure 18 illustrates the steps involved in conducting each experiment, representing a cyclical process.

Figure 18 - Experimental procedure.

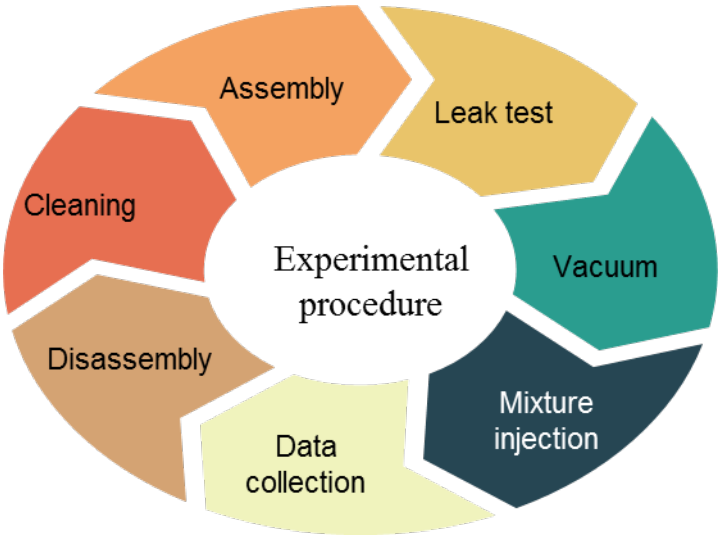

Source: Created by the author (2024).

4.3 Mixtures preparation

Preparing the hydrocarbon liquid binary mixture involves progressively increasing the molar amount of n-hexadecane. The mixture was combined with four different n-hexadecane contents: 20.2%, 40%, 60%, and 80% molar, as given in Table 4. Once the binary mixture was prepared the fluid phase behavior was investigating by addition of CO_2 with a global mole composition ranging from 20 until 98 mol% CO_2.

Table 4 - Molar fractions of binary-hydrocarbon mixtures

Acronym*	**Molar fraction mol/mol**	
	n-$C_{10}H_{22}$	**n-$C_{16}H_{34}$**
M-20	0.789	0.202
M-40	0.600	0.400
M-60	0.400	0.600
M-80	0.200	0.800

*Acronym based on n-hexadecane composition.
Source: Created by the author (2024).

By following this methodology, Eq 13 was used to combine all uncertainty source and the global mole fraction $\left(x_{CO_2}\right)$ combined uncertainty was determined.

$$u_c\left(x_{CO_2}\right) = x_{CO_2}\left(-x_{CO_2}\right)\left(\frac{u^2\left(m_{CO_2}\right)}{m_{CO_2}^2} + \frac{u^2\left(m_{liq}\right)}{m_{liq}^2}\right)^{1/2} \qquad (13)$$

Where the $u\left(m_{CO_2}\right)$ and $u\left(m_{liq}\right)$ represent the standard uncertainties of ± 0.01 g and ±0.005 g, respectively.

To conduct phase transition measurements, it is essential to follow a series of stability criteria and procedures to ensure the system's stability. First, the temperature is homogenized until the desired set point is reached. During this process, constant stirring is maintained while pressurizing at a rate of 2 MPa/min to achieve a homogeneous single-phase mixture.

Before starting the depressurization, stability criteria are verified. These criteria ensure that, over a period of 5 minutes, the volume variation does not exceed 0.05 ml, and the temperature variation remains below 0.5 K. Once these criteria are met, the depressurization is carried out at a controlled rate of 0.1 MPa/min through an isothermal process until a phase transition is observed. This transition may be liquid-vapor (L→L+V), liquid-liquid (L→L+L), or liquid-liquid-vapor (L+L→L+L+V), allowing the determination of the corresponding phase transition values. Figure 19 outlines the CCE test methodology:

Figure 19 - Methodology adopted for constant composition expansion tests, where *Pi* is the initial test pressure (single-phase system), *Ti* the initial test temperature and the subscript 1 is the experiment temperature.

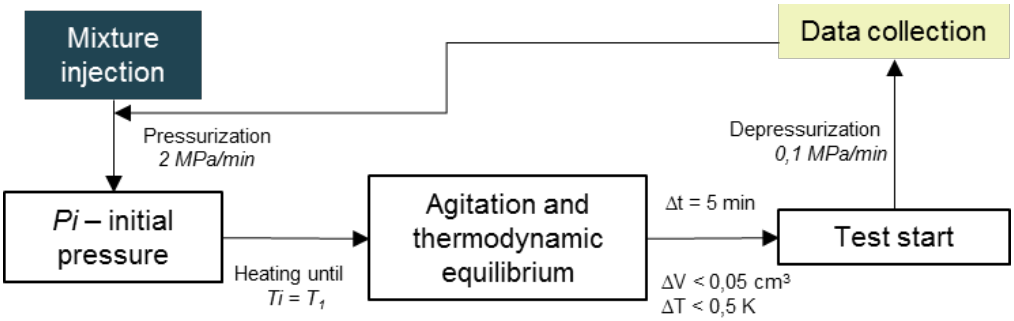

Source: Adopted from (da Costa *et al.*, 2024).

According to the Guide of Uncertainty Measurement (GUM) of the National Institute of Standards and Technology (Taylor, B.; Kuyatt, C., 1994), the uncertainties for pressure transition *u(p)* for all the transition phenomena observed were calculated by Eq.14.

$$u^2(p) = u^2(p^{gauge}) + u^2(p^{obs}) + \left[\left(\frac{\partial p}{\partial T}\right) u(T^{gauge})\right]^2 + \left[\left(\frac{\partial p}{\partial x_{CO_2}}\right) u(x_{CO_2})\right]^2 \qquad (14)$$

Where the uncertainties for phase change observations [$u(p^{obs})$] equals 0.02 MPa, temperature gauge $u(T^{gauge})$ equals 0.1 K, and pressure gauge [$u(p^{gauge})$] equals 0.02 MPa.

4.4 Thermodynamics modeling

4.4.1 Peng Robinson's equation of state

PR's equation of state (Peng; Robinson, 1976) presented in Eq. 12 was used to model all fluid-fluid transition experimentally measured. The criterion for establishing phase equilibrium is ensuring the fugacity of each component. The attraction parameters a and co-volume b were estimated using quadratic and linear mixing rules given by Eqs. 15 and 16, respectively.

$$a = \sum_i \sum_j x_i x_j \sqrt{a_i a_j}\,(1 - k_{ij}) \qquad (15)$$

$$b = \sum_i x_i b_i \qquad (16)$$

Where x_i is the molar fraction of the component i, and x_j is the molar fraction of the component j, and k_{ij} is the binary interaction parameter between components *i* and *j*.

Each parameter (a_i) and (b_i) for the PR EOS are calculated according to Eqs 17 and 18, respectively. These components are a function of the critical temperature Tc_i and critical pressure *Pci* of the components in the mixtures.

$$a_i = 0.45724 \frac{(RTc_i)^2}{Pc_i} \alpha_i(T) \qquad (17)$$

$$b_i = 0.0778 \frac{RTc_i}{Pc_i} \qquad (18)$$

The attraction parameter that describes the temperature dependence is characterized by Eq. 19, as follows:

$$\alpha_i(T) = \left(1 + m_i\left(1 - \sqrt{\frac{T}{Tc_i}}\right)\right)^2 \qquad (13)$$

The form factor (m_i) for PR EOS is derived from the acentric factor (ω_i), as presented in Eqs. 20 and 21.

$$m_i = 0.37464 + 1.54226\omega_i - 0.26992\omega_i^2 \; for \; \omega_i < 0.49 \qquad (20)$$

$$m_i = 0.379642 + 1.48503\omega_i - 0.164423\omega_i^2 + 0.01666\omega_i^3 \; for \; \omega_i \geq 0.49 \qquad (21)$$

4.4.2 Binary interaction coefficients (kij)

The significance of binary interaction coefficients (k_{ij}) has been highlighted in the literature regarding the precision of fluid phase behavior equation of state prediction. These coefficients theoretically represent interactions between different molecules, with their values

typically derived by aligning predicted saturation pressure curves with experimental data (Peng; Robinson, 1976).

The values of k_{ij} for all possible binary pairs are obtained by fitting the experimental vapor-liquid equilibrium data of the mixtures. This approach, however, limits the predictive ability of the equation (Gao *et al.*, 1992).

4.4.2.1 CO_2/decane

Binary interaction parameters k_{ij}, temperature dependent for the CO_2/decane pair were determined through a trial-and-error process, using experimental data obtained in the laboratory for the binary system. To determine the optimal parameters of the ELV model, objective functions (OF) are employed as iterative procedures. These allow optimal values to be calculated using explicit models, since the adjusted variables are obtained from an algorithm for calculating the bubble point pressure (López; Trejos; Cardona, 2006). In the present work, 16 binary mixtures were analyzed, and the minimization of the following objective function was applied to calculate the system parameters at each temperature studied.

For systems composed of CO_2, the objective function used to determine the binary interaction considers both the bubble pressure and the compositions of the vapor phase at the bubble point, as described below:

$$E_{Pi} = \left(\frac{P^{cal} - P^{exp}}{P^{exp}}\right)_i \qquad (22)$$

$$E_{yi} = \left(y_1^{cal} - y_1^{exp}\right)_i \qquad (23)$$

Where *P* represents the saturation pressure, y_1 is the composition of component 1 in the vapor phase, and *E* corresponds to the error between the calculated and experimental values. The superscript *cal* indicates the data calculated through the Peng Robinson equation, while *exp* refers to the experimental data. The regression is performed by minimizing the objective function:

$$OF = \sum_{i=1}^{Np} \left[\frac{P_i^{cal} - P_i^{exp}}{P_i^{exp}} \right]^2 + \sum_{i=1}^{Np} \left[y_1^{cal} - y_1^{exp} \right]^2 \qquad (24)$$

In which the summation is done over the number of experimental points (Np).

4.4.2.2 CO_2/hexadecane

In a similar way to the case of the binary interaction parameter of the CO_2/decane system, obtaining the temperature-dependent binary interaction parameter was implemented for the CO_2/hexadecane system, due to the increase in the deviation observed as the temperature decreases.

In this case, bubble pressure data are not available for the binary system, so information available in the literature was used, specifically solubility data. A total of 37 solubility data were used (Charoensombut-amon; Martin; Kobayashi, 1986) at temperatures of 323.15 K, 313.15 K and 308.15 K. To determine the model parameters, the calculation using the isothermal flash method was used as an objective function, the detailed explanation of which is presented in the following section.

The relationship between binary interaction and temperature was established. Table 5 summarizes the binary interaction parameters used in this study:

Table 5 - Binary interaction parameters as a function of temperature for the binary system CO_2/hexadecane.

Temperatura (K)	**k_{ij} (CO_2/n-$C_{16}H_{34}$)**	**Function of temperature**
283.15	0.11405	
298.15	0.10911	$-3.29X10^{-4} \cdot T[°C] + 0.117337$
323.15	0.10127	

Source: Created by the author (2024).

In this work, the binary interaction parameters were determined for the two pairs: CO_2/n-$C_{10}H_{22}$ and CO_2/n-$C_{16}H_{34}$, as demonstrated in the previous sections using the Peng-

Robinson equation. For the hydrocarbon pair n-$C_{10}H_{22}$/n-$C_{16}H_{34}$, it is worth noting that the binary interaction parameters are generally zero or very close to zero, which is why many authors assume a value of zero (Gao *et al.*, 1992; Pedersen; Thomassen; Fredenslund, 1985). Therefore, a value of zero was adopted in this study.

Pure carbon dioxide properties were taken from references available in NIST webbook database. Moreover, decane and hexadecane properties are taken from the literature (Ambrose; Tsonopoulos, 1995). All data are summarized in Table 6.

Table 6 - Properties of pure compounds considered in this work.

Component	***Pc*/MPa**	***Tc*/K**	***ω***	**MW/[kg/kmol]**
CO_2	7.383	304.21	0.2236	44.01
n-$C_{10}H_{22}$	2.110	617.7	0.4923	142.29
n-$C_{16}H_{34}$	1.489	717	0.742	226.44

Source: Created by the author (2024).

All calculations were performed using the software SPECS version 5.63 (da Costa *et al.*, 2024; Ferreira *et al.*, 2018), developed by the Center of Energy Resources and Engineering at the Denmark Technical University (CERE–DTU).

4.4.3 Method of Isothermal Flash

Miscible gas flooding in oil reservoirs can be modeled using isothermal flash calculations. The conventional approach assumes the number of phases present at equilibrium and estimates initial values for the equilibrium factors. Flash calculations consider iteratively determining the compositions and quantities of the phases present in a mixture under specific pressure and temperature conditions. By comparing fugacities and using phase stability criteria, it is possible to identify if a new phase has formed. Newton-Raphson method has been employed as a procedure for this method (Henderson *et al.*, 2001; Michelsen, 1982a, 1982b).

The traditional approach assumes the number of phases in equilibrium and initializes the equilibrium factors. Subsequently, the material balance equations are solved to

determine the fractions and compositions of the phases, updating the balance factors iteratively until convergence is achieved. This process allows calculating the amount of each component in each phase and the proportion of each phase present in the mixture. Once the thermodynamic formulation is established, a suitable minimization algorithm is selected to find the global minimum of the Gibbs free energy (Henderson *et al.*, 2001).

The equilibrium state is defined as the one in which the minimum of the Gibbs free energy is reached, considering the possible configurations of the system under constant conditions of temperature and pressure. In the case of a vapor-liquid system, the total Gibbs free energy is expressed by the following equation:

$$G = \sum_{i=1}^{r} n_i^{(v)} \mu_i^{(v)} + \sum_{i=1}^{r} n_i^{(l)} \mu_i^{(l)} \qquad (25)$$

Where $n_i^{(f)}$, f= v, l, represents the number of moles of component *i* in the vapor phase $n_i^{(v)}$or liquid $n_i^{(l)}$phase and μ represent the chemical potential.

According to the minimum Gibbs free energy principle, in the equilibrium state, the intensive parameters of a system correspond to the values that minimize the total molar Gibbs free energy, keeping the specified temperature and pressure constant. In the SPECS software, a flash calculation is performed at the temperature and pressure of each experimental point. The experimental phase compositions are compared with the predictions. The equilibrium factors Eqs. 26 and 27 represent the concentrations of each component in the different phases (KNUDSEN, Kim; POULSEN, Thomas, 2009).

$$R_{1i} = ln\left(\frac{y_1^c}{x_1^c}\frac{x_1^e}{y_1^e}\right)_i \qquad (26)$$

$$R_{2i} = ln\left(\frac{y_2^c}{x_2^c}\frac{x_2^e}{y_2^e}\right)_i \qquad (27)$$

where:

y_i: molar composition of component *i* in the vapor phase.

x_i: molar composition of component i in the liquid phase.

c: calculated point.

e: experimental point.

5 RESULTS AND DISCUSSION

5.1 Data validation and reproducibility

The fluid-fluid transition experimentally measured in this work for CO_2 + decane are given in Table 7. These values are used as a method validation by comparing with experimental data available in literature.

Table 7 - Experimental data of bubble points at different global compositions of CO_2(1). Binary system: CO_2 (1) + decane.

x_1	T/K	P/MPa	x_1	T/K	P/MPa
0.3280	298.09	2.40	0.3150	283.55	2.21
	323.08	3.14	0.5360	283.82	3.38
0.4950	298.28	4.03	0.7160	283.69	4.08
	322.96	5.51	0.9000	283.43	4.28
0.7770	298.07	5.50	0.9510	283.66	4.39
	323.21	8.57	0.9820	283.75	4.51
0.9110	298.03	5.87			
	323.01	9.47			
0.9790	323.29	9.73			
0.9890	298.39	6.35			
	322.68	9.57			

Source: Created by the author (2024).

Figure 20 presents the method validation by comparing data from the literature at different temperatures T = (283.15, 298.15, and 323.15) K, with transition pressures ranging from 0.2 to 10 MPa. Typically, the most experimental data available in the literature for CO_2 + decane are given at temperature condition higher than T = 313.15 K. ¬The comparation was performed by using binary system with a global mole composition of 30 to 98.9 mol % CO_2. All these data are represented by the reference works correspond to these compositions.

Figure 20 - Comparison between experimental, bubble point (circle, o) and literature data for carbon dioxide + decane binary system in pressure at different global mole composition. Reamer & Sage, 1963 (triangle, Δ). Jiménez-Gallegos et al., 2006 (cross, x). Nascimento et al., 2019 (rectangle, □). T = 323.15 K (red dashed line, ---), T = 298.15 K (blue dashed line, ---), and T = 283.15 K (green dashed line, ---).

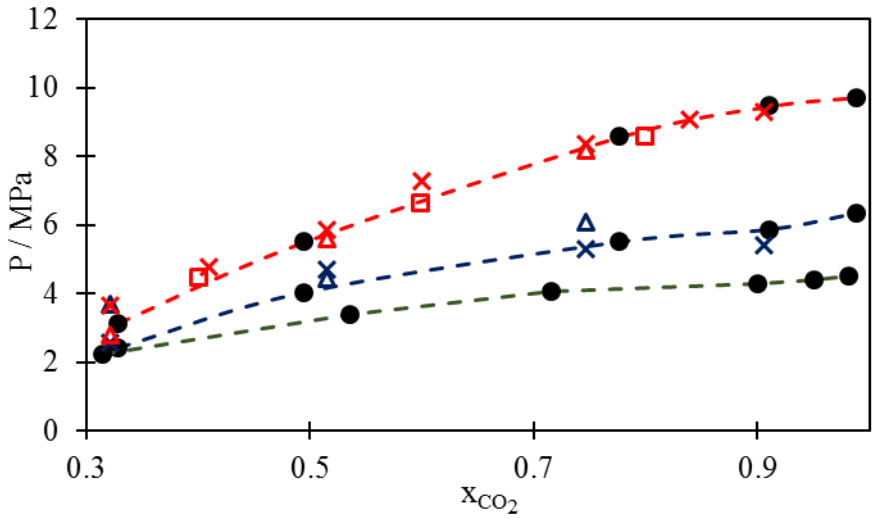

Source: Created by the author (2024).

Once the experimental data available in the literature were not measured at the same temperature as this work, the data from the literature were interpolated for the temperatures studied. However, for the temperature of 283.15 K, it was not possible to interpolate because there are no articles that study temperatures between these values.

Nevertheless, for temperatures of 298.15 K and 323.15 K, the points showed great accuracy with the experimental data. It is important to note that the article by Reamer & Sage from 1963 (Reamer; Sage, 1963) has significant variance. Moreover, these results are also in line with the low expanded uncertainty calculated for the overall molar composition for CO_2 + decane mixtures, which was less than u(xi) = 0.7 mol%.

5.2 CO_2 + decane + hexadecane systems

In the following sections, the tables and figures corresponding to the experimental data of the ternary systems CO_2 + decane + hexadecane are presented, together with the curves obtained by modeling using the Peng-Robinson equation of state. For these systems, the phase transitions observed include vapor-liquid, liquid-liquid, and vapor-liquid-liquid.

5.2.1 CO_2 (1) + M-20 ternary system

Table 8 shows the fluid-fluid phase transitions observed at three different temperatures for various mixtures with overall CO_2 compositions in the ternary system CO_2 + M-20.

Table 8 - Fluid-fluid transition pressure at a temperature T in different mixtures of global composition x_{CO_2} with its expanded (k = 2) uncertainty U(p) for CO_2 (1) + M-20 ternary system.

T/K	P/MPa	U(p)	transition	T/K	P/MPa	U(p)	transition
	x_1= 0.2250 ± 0.0093				x_1 = 0.4290 ±0.0046		
298.39	1.83	0.1	L-VL	298.37	3.69	0.07	L-VL
323.44	2.51	0.12	L-VL	323.64	5.06	0.08	L-VL
	x_1 = 0.6300 ± 0.0020				x_1 = 0.8130 ± 0.0009		
298.34	5.1	0.06	L-VL	283.84	4.27	0.06	L-VL
323.37	7.4	0.06	L-VL	298.41	5.87	0.06	L-VL
				322.79	9.28	0.06	L-VL
	x_1 = 0.8760 ± 0.0008				x_1 = 0.9500 ± 0.0006		
284.11	4.35	0.06	L-VL	283.99	4.41	0.06	L-VL
298.37	5.96	0.06	L-VL	299.19	6.22	0.06	L-VL
323.05	9.77	0.06	L-VL	323.14	10.36	0.06	V-LV
	x_1 = 0.9870 ± 0.0007						
283.23	4.64	0.06	L-VL				
298.83	6.39	0.06	L-VL				
322.7	10.35	0.07	V-LV				

Source: Created by the author (2024).

Figure 21 presents the P-x diagram of the M-20 mixture with addition of CO_2. Similar trends of bubble points were observed for all the temperatures investigated. Two dew points were identified at compositions greater than 95 mol% CO_2 for T = 323.5 K. As it has a higher percentage of the lighter hydrocarbon (decane), the results are similar to those determined by (Jiménez-Gallegos; Galicia-Luna; Elizalde-Solis, 2006) at T = 319.11 K and (Nascimento *et al.*, 2019) at T = 313.2 K for CO_2 + decane binary system. This shows that the mixture with an excess of decane, specifically with 80% in the hydrocarbon fraction, exhibits a behavior similar to that of the binary mixture CO_2 + decane.

Figure 21 - Px diagram for different mixtures of CO_2 global mole composition CO_2 (1) + M-20. Bubble point (triangle, Δ); dew point (diamond, ◊). The solid line (—) represents modeling with PR.

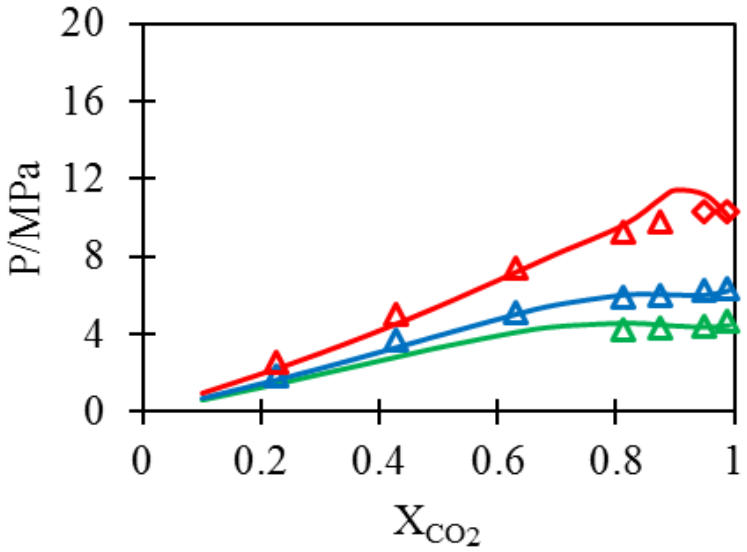

Source: Created by the author (2024).

In addition, this isothermal phase behavior was modeled using the Peng-Robinson equation of state with its classical mixing rules. As shown in Figure 21, there are no significant differences from the experimental values. The P-x graph was obtained through successive calculations at different compositions to determine the bubble points of the system. However, multiple flash calculations were performed for the dew point results to determine the pressure at which two phases are obtained.

5.2.2 CO_2 (1) + M-40 ternary system

Table 9 shows the fluid-fluid phase transitions observed at three different temperatures for various mixtures with overall CO_2 compositions in the ternary system CO_2 + M-40.

Table 9 - Phase equilibria data, fluid-fluid transition pressure at a temperature T in different mixtures of global composition x_{CO_2} with its expanded (k = 2) uncertainty U (p) for CO_2 (1) + M-40 ternary system.

T/K	P/MPa	U(p)	transition	T/K	P/MPa	U(p)	transition
	x_1 = 0.4100 ±0.0069				x_1 = 0.6180 ± 0.0034		
298.48	3.45	0.08	L-VL	298.81	5.16	0.06	L-VL
323.56	4.61	0.11	L-VL	323.26	7.25	0.07	L-VL
	x_1 = 0.797 ± 0.0011				x_1 = 0.9020 ± 0.0006		
298.41	6.01	0.06	L-VL	283.88	4.96	0.06	L-LL
323.54	9.61	0.06	L-VL	283.9	4.41	0.06	LL-LLV
				298.95	6.21	0.06	L-VL
				323.15	11.21	0.07	L-VL
	x_1 = 0.9220 ± 0.0004				x_1 = 0.9500 ± 0.0003		
283.92	4.99	0.06	L-LL	284.45	4.69	0.06	L-LL
283.92	4.44	0.06	LL-LLV	284.45	4.48	0.06	LL-LLV
299.06	6.24	0.06	L-VL	298.24	6.39	0.07	L-VL
322.94	11.49	0.07	L-VL	322.88	11.73	0.07	V-LV
	x_1 = 0.9850 ± 0.0005						
284.37	4.41	0.07	L-VL				
298.11	6.3	0.07	L-VL				
323.07	11.25	0.07	V-LV				

Source: Created by the author (2024).

In Figure 22, on the left, the P-x diagram of the M-40 mixture with the addition of CO_2 is presented. The observed behavior is similar to that of the previous system for T=298.15 and 323.15 K, without significant variations in the bubble point values. However, as can be seen on the right side of the figure, with a closer look at the values obtained, from a global composition of 90.2 mol% of CO_2, a phase heterogeneity assigned to a liquid to liquid-liquid transition at T=283.15K.

Furthermore, when the pressure decreases, the liquid-liquid equilibrium evolves into a three-phase liquid-liquid-vapor equilibrium, as shown in the figure. The difference in the transition pressure from LL to LLV has an approximate value of 0.5 MPa, significantly low compared to the transitions observed in other studied systems. However, the LLV transition pressure is generally close to the saturation pressure of CO_2 at the same temperature.

Additionally, once this mixture is not a real binary mixture, the LLV region is not monovariant and it occurs in a narrow region of the phase diagram. Nevertheless, when mixture with 98.5 mol% CO_2 was studied at 283.15 K, no liquid-liquid equilibrium was detected, and a typical biphasic liquid-vapor equilibrium was observed. This result shows a critical curve

enclosing the liquid-liquid region, rising to a liquid-vapor transition when the binary system is studied with a higher CO_2 gas content.

Figure 22 - Px diagram for different mixtures of CO_2 global mole composition CO_2 (1) + M-40. Bubble point (triangle, Δ); dew point (diamond, ◊); liquid-liquid balance (cross, ×); liquid-liquid-vapor (circle, ○). The solid line (—) represents modeling with PR.

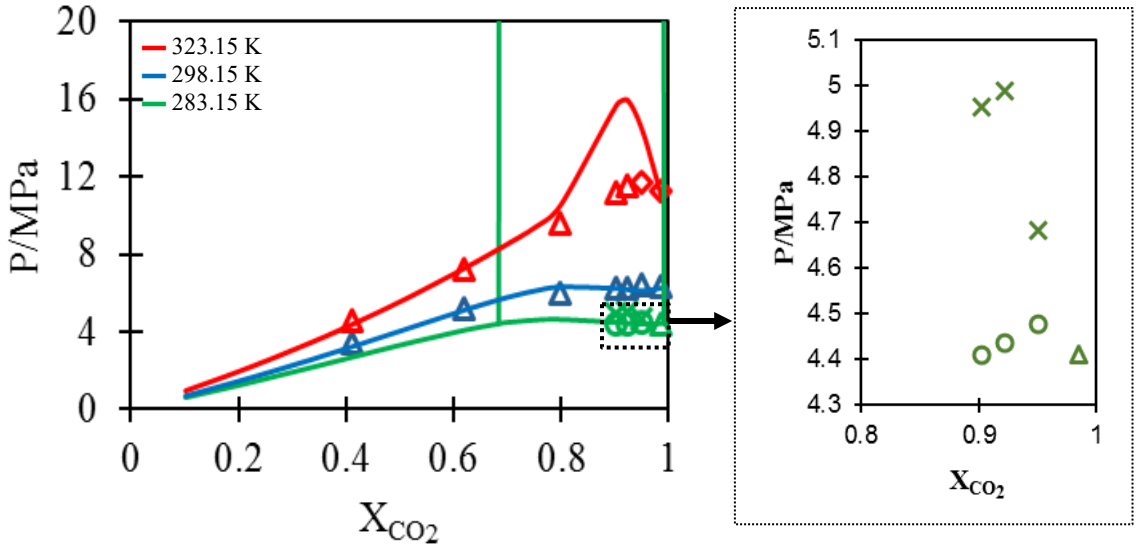

Source: Created by the author (2024).

At this stage of model development, discrepancies with experimental results begin to emerge. Experimentally, complex phenomena are observed due to the increase in the composition of n-hexadecane in the system, such as phase transitions from liquid to liquid-liquid and from liquid-liquid to liquid-liquid-vapor at 283.15 K.

In the modeling, the software fails to determine the points where the system is monophasic, obtaining only the LLV points in the diagram through the flash method. The result is two lines on the right and left that delimit the section where the liquid-liquid region is predicted. A discrepancy is observed between the predictive results and the bubble and dew points at 323.15 K. This can be attributed to the increased asymmetry in the system and the pressure and temperature conditions being above the critical conditions of the CO_2 component. Additionally, experimentally determining where the phase transition occurs becomes more complex under supercritical conditions.

Figure 23 shows photographs of the depressurization process conducted on the system with a composition of 90.2 mol % CO_2 at 283.15 K. The pressure difference between the LL to LLV transition is remarkably low compared to the pressure deltas observed in other

systems. The pressure values recorded by the pressure transducer are displayed below each photograph in bar units (equipment units). The LLV point was identified by the appearance of the first bubble visible in the cameras, highlighted with a red circle in the third photograph of Figure 23.

Figure 23 - Image sequence of the depressurization of the system with 90.2 mol % CO_2 + M40.

Source: Created by the author (2024).

According to (Quiñones-Cisneros, 1997), the Peng-Robinson (PR) equation predicts a type III phase diagram for CO2 + n-alkane mixtures following the Scott and van Konynenburg classification (Van Konynenburg, P. H.; Scott R. L., 1980), starting from the binary mixture CO_2 (component 1) + n-C_{10} (component 2). However, experimental observations show immiscibility only below T = 273.15 K for this system. This behavior has been described by (Kukarni *et al.*, 1974) for CO_2 + decane mixtures along their multiphase loci, demonstrating immiscibility at low temperatures, including LLV regions. Moreover, according to (Schneider *et al.*, 1967) the miscibility of n-decane, n-undecane, and probably dodecane with CO_2 in the liquid phase is so good that separating into two liquid phases would only occur at very low temperatures.

Therefore, based on the experimental results reported in the literature, it is concluded that within the CO_2 + n-alkane series, the transition from Type II to Type III phase behavior occurs in the CO_2 + n-tridecane systems. This implies that CO_2 + n-C_{14} and higher systems exhibit Type III phase behavior (Fall; Fall; Luks, 1985; Fall; Luks, 1984; Hottovy; Luks; Kohn, 1981).

In this work, it was observed that the ternary system studied, at the analyzed compositions, shows Type III behavior. This phenomenon can be attributed to the presence of hexadecane, as binary systems with decane do not exhibit this type of behavior.

5.2.3 CO_2 (1) + M-60 ternary system

Table 10 presents the fluid-fluid phase transitions observed at three different temperatures for various mixtures with global compositions of the CO_2 + M-60 ternary system.

Table 10 - Phase equilibria data, fluid-fluid transition pressure at a temperature T in different mixtures of global composition x_{CO_2} with its expanded (k = 2) uncertainty U (p) for CO_2 (1) + M-60 ternary system.

T/K	P/MPa	U(p)	transition	T/K	P/MPa	U(p)	transition
x_1 = 0.2090 ± 0.0097				x_1 = 0.4200 ± 0.0060			
283.71	1.86	0.11	L-VL	298.14	3.63	0.07	L-VL
298.42	2.62	0.07	L-VL	323.14	4.89	0.09	L-VL
323.14	2.88	0.11	L-VL				
x_1 = 0.6090 ± 0.0028				x_1 = 0.8070 ± 0.0007			
298.91	5.3	0.07	L-VL	284.25	7.94	0.06	L-LL
322.77	7.31	0.1	L-VL	284.25	4.43	0.06	LL-LLV
				298.69	6.23	0.06	L-VL
				322.54	10.42	0.06	L-VL
x_1 = 0.8980 ± 0.0007				x_1 = 0.9530 ± 0.0004			
284.25	4.49	0.06	LL-LLV	284.47	4.53	0.06	LL-LLV
298.41	10.43	0.06	L-LL	298.58	10.57	0.06	L-LL
298.41	6.24	0.06	LL-LLV	298.58	6.29	0.06	LL-LLV
322.49	12.65	0.06	L-VL	322.52	16.7	0.06	V-LV
x_1 = 0.9850 ± 0.0003							
283.77	8.23	0.06	L-LL				
283.69	4.47	0.06	LL-LLV				
298.59	8.05	0.07	L-LL				
298.55	6.36	0.06	LL-LLV				
322.98	12.8	0.07	V-LV				

Source: Created by the author (2024).

The P-x diagram of the M-60 mixture with the addition of CO_2 is shown in Figure 24. In this system, at T = 298.15 K, bubble points were observed at low global CO_2 compositions. Starting from a composition of 89.8 mol% CO_2, the system initially presented as a monophasic liquid, which evolved into a liquid-liquid equilibrium (LLE) as the pressure

decreased. At this point, the increase in n-hexadecane in the mixture resulted in the appearance of the LL region in the phase diagram at 298.15 K. Additionally, during isothermal depressurization in the liquid-liquid region, another phenomenon was observed: a mass barotropic inversion, also known as density inversion (Quinteros-Lama *et al.*, 2015).

On the other hand, the team of (Charoensombut-amon; Martin; Kobayashi, 1986) observed this phenomenon in the binary system n-hexadecane + CO_2 at a pressure of 13.89 MPa and a temperature of 308.15K. Moreover, (Simoncelli *et al.*, 2020) observed this phenomenon in the binary system at a composition of 90.98 mol% CO_2 with hexadecane at a temperature of 298.1 K. For this knowledge, there are no studies on phase behavior for ternary systems mixtures with n-paraffins exhibiting this phenomenon.

Figure 24 - Px diagram for different mixtures of CO_2 global mole composition CO_2 (1) + M-60. Bubble point (triangle, Δ); dew point (diamond, ◊); liquid-liquid balance (cross, ×); liquid-liquid-vapor (circle, ○). The solid line (—) represents modeling with PR.

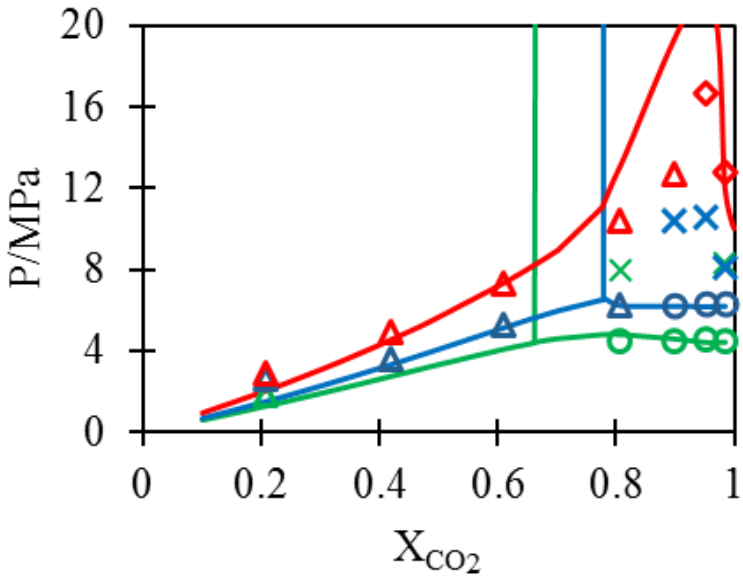

Source: Created by the author (2024).

For this system, at temperatures of 283.15 and 298.15 K, the model fails to obtain pressure values at which the system is entirely monophasic in the liquid state. Therefore, as shown in Figure 24, vertical lines with a tendency towards infinite pressures are presented, which delimit the section from which the model does not identify phase behavior, including ELL, ELLV and barotropic inversion.

Figure 25 presents a series of images captured during isothermal depressurization CO_2 (1)/decane (2) /hexadecane (3) at 298.15 K with a composition of: x_1=0.90, x_2=0.02, x_3=0.08. Each imagine represents:

a) At pressures above 15.8 MPa, the system presents a monophasic liquid;

b) At pressure 15.8 MPa, the value of the transition to liquid-liquid was recorded, where a change in color is seen;

c) At a lower pressure of this value, it is possible to see the liquid L_1 dispersed in the second liquid L_2;

d) Constant depressurization

e) At constant depressurization, the system presents the phenomena of density inversion at a pressure above 9 MPa;

f) At a pressure of about 6 MPa, the system presents LLV; the image shows the three phases at pressures lower than this value.

Figure 25 - Isothermal depressurization of the system CO_2 (1)/decane (2) /hexadecane (3) at 298.15 K with a composition of: x_1=0.90, x_2=0.02, x_3=0.08. a) Monophasic liquid; b) transition of liquid to liquid-liquid; c) L_1 dispersed in L_2; d) depressurization; e) density inversion and f) liquid-liquid-vapor.

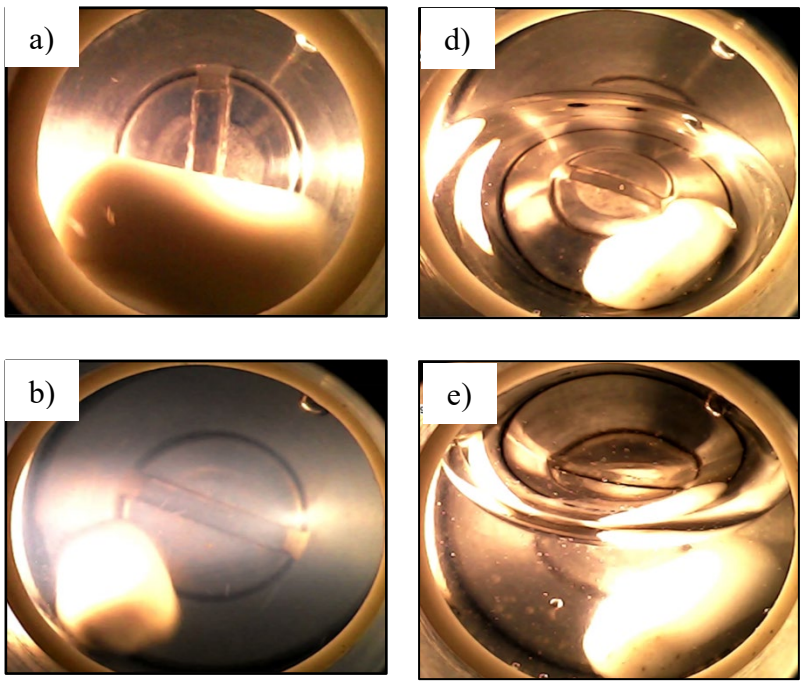

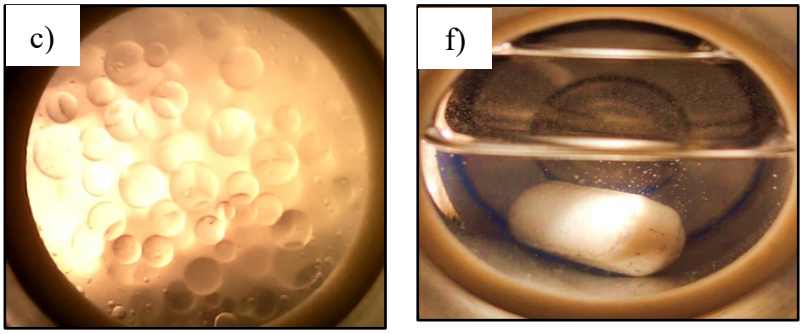

Source: Created by the author (2024).

5.2.4 CO_2 (1) + M-80 ternary system

Table 11 presents the fluid-fluid phase transitions observed at three different temperatures for various mixtures with global compositions of the CO_2 + M-80 ternary system.

Table 11 - Phase equilibria data, fluid-fluid transition pressure at a temperature T in different mixtures of global composition x_{CO_2} with its expanded (k = 2) uncertainty U (p) for CO_2 (1) + M-80 ternary system.

T/K	P/MPa	U(p)	transition	T/K	P/MPa	U(p)	transition
x_1 = 0.2370 ± 0.010				x_1 = 0.4280 ± 0.0059			
298.43	2.19	0.14	L-VL	283.96	3.53	0.06	L-VL
323.12	2.44	0.2	L-VL	298.22	4.57	0.08	L-VL
				323.09	6.19	0.11	L-VL
x_1 = 0.6110 ± 0.0028				x_1 = 0.8000 ± 0.0007			
283.35	4.29	0.07	L-VL	283.24	4.47	0.07	LL-LLV
298.4	5.79	0.06	L-VL	298.55	7.74	0.06	L-VL
323.17	8.57	0.07	L-VL	322.94	11.06	0.06	L-VL
x_1 = 0.9000 ± 0.0006				x_1 = 0.9490 ± 0.0006			
283.11	4.45	0.06	LL-LLV	283.46	4.51	0.06	LL-LLV
298.33	15.78	0.06	L-LL	298.32	14.39	0.07	L-LL
298.33	6.44	0.07	LL-LLV	298.32	6.52	0.07	LL-LLV
323.16	14.73	0.07	L-VL	323.03	14.65	0.06	V-LV
x_1 = 0.9800 ± 0.0004							
283.44	13.3	0.06	L-LL				
283.38	4.49	0.06	LL-LLV				
298.14	10.38	0.08	L-LL				
298.3	6.37	0.08	LL-LLV				
323.11	14.46	0.07	V-LV				

Source: Created by the author (2024).

Figure 26 illustrates the phase behavior of the CO_2 + M80 system at various global CO_2 compositions. The system's complexity is emphasized, with 80 mol % of the mixture being

n-hexadecane in the binary hydrocarbon liquid mixture. As a result, an immiscibility window (liquid-liquid) appears at higher pressures, with the highest experimental point observed at 16 MPa. This contrasts with the previous CO_2 + M60 system, which showed immiscibility at around 11 MPa at a temperature of 298.15 K and a composition of approximately 90mol % CO_2.

Figure 26 - Px diagram for different mixtures of CO_2 global mole composition CO_2 (1) + M-80. Bubble point (triangle, Δ); dew point (diamond, ◊); liquid-liquid balance (cross, ×); liquid-liquid-vapor (circle, ○). The solid line (—) represents modeling with PR.

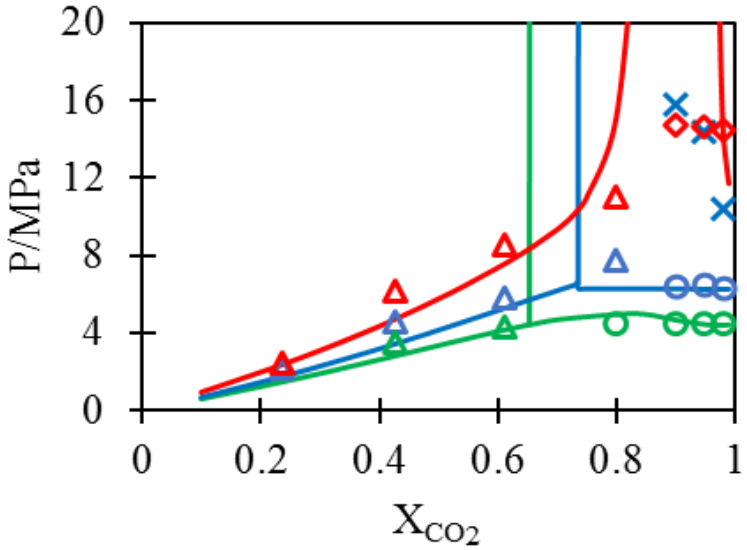

Source: Created by the author (2024).

Predicting phase behavior at this stage becomes increasingly complex. Consequently, the graph delineates with vertical lines the region where a liquid-liquid to liquid-liquid-vapor transition is observed at temperatures of 283.15 and 298.15 K, as shown in the previous section, due to the model's inability to identify a single-phase liquid region at any pressure value. The same situation is perceived at a temperature of 323.15 K, where there is an interval in which a single-phase section is not identified in the system. The prediction of the VLLE region was carried out using the isothermal expansion method.

The same barotropic inversion behavior was detected for the M-80 mixture when the system was studied with high CO_2 gas content. As shown in the sequence of images in Figure 25, photos d and e illustrate the barotropic inversion. This inversion occurs over a range of pressures at a constant temperature, making it difficult to pinpoint the exact pressure at which

isopicnicity - equality of densities - occurs, thus introducing a significant margin of error. However, this phenomenon is observed within a pressure range of 8 to 9 MPa for both systems (CO_2 + M-60 and CO_2 + M-80) without a significant variation in the pressure at which the inversion occurs.

For instance, the experimental pressure points recorded when a gravitational change in the position of the liquids was observed were 8.04 MPa for CO_2 + M-60 and 8.82 MPa for CO_2 + M-80, both at a composition of 90 mol% CO_2.

5.2.5 Influence of hexadecane on the phase behavior of the ternary system CO_2+decane+hexadecane

Figure 27 illustrates the influence of hexadecane on the phase behavior of the ternary system CO_2 + decane + hexadecane at different temperatures: a) 283.15 K, b) 298.15 K, and c) 323.15 K. The addition of a longer-chain compound increases the complexity of the system, which can be attributed to an increase in asymmetry and more intricate interactions involving CO_2 molecules. As a result, the liquid-liquid region expands to a broader pressure range as the content of n-hexadecane increases in the system, particularly at temperatures of 283.15 and 298.15 K. However, the pressure corresponding to the LLV equilibrium at each studied temperature remains constant across the analyzed systems, as this value is directly related to the vapor pressure of CO_2 at that temperature.

Figure 27 - P-x diagrams illustrating the phase behavior for different mixtures of the CO_2 + decane + hexadecane system at different mol fractions of hexadecane in the binary liquid system: ◊ M-20; x M-40; □ M-60; o M-80. The values of hexadecane + CO_2 binary system from the literature are showed: Simoncelli et al., 2020 (red triangle, Δ). a) 283.15 K; b) 298.15 K; c) 323.15 K.

a) b)

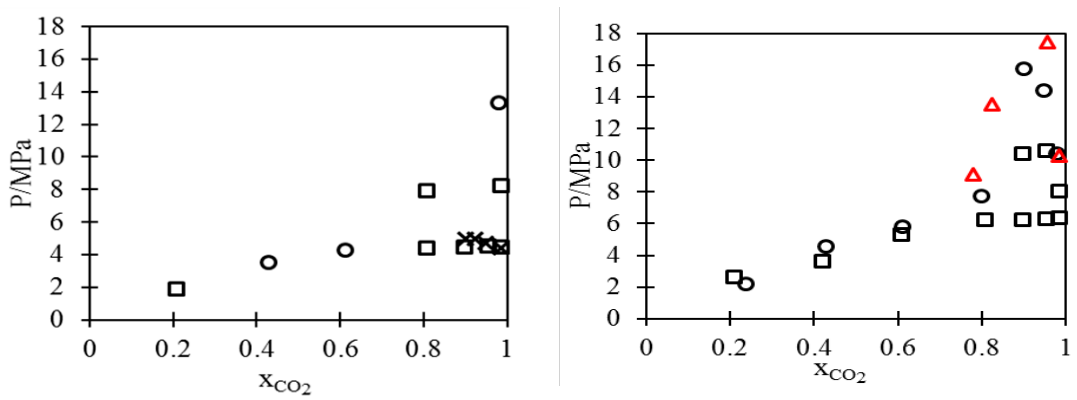

c)

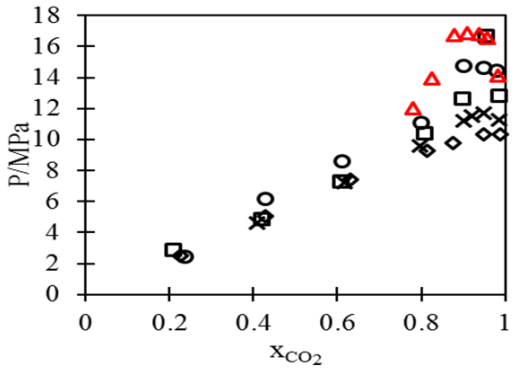

Source: Created by the author (2024).

The analysis of Figure 27c shows that the transition pressures of the binary system CO_2 + hexadecane are higher than those of the ternary systems CO_2 + decane + hexadecane at different compositions at 323.15 K. In addition, a progressive increase in the content of n-hexadecane raises the saturation points. At temperatures of 298.15 K and 283.15 K, shown in Figures 27a and 27b, complex transitions appear with the increase of n-hexadecane in the ternary mixture, including transitions from liquid to liquid-liquid and from liquid-liquid to liquid-liquid-vapor. This shows that decane dissolves in CO_2 more than hexadecane.

With the high solubility of decane in CO_2, an increase in the hexadecane composition in the ternary mixture raises the transition pressure for a single-phase liquid system, especially for compositions with a high CO_2 content, around 80% in molar fraction. As a result, the greater asymmetry of the system causes immiscibility windows to form at pressures and temperatures where they were not present before.

At low temperatures, approximately 298.15 K and 283.15 K, the increased concentration of CO_2 in the liquid phase significantly alters the system's density and intermolecular interactions. Since the 1960s, when studies on phase behavior in carbon dioxide-hydrocarbon systems began, it has been observed that the density of the liquid saturated with carbon dioxide increases (Kariznovi; Nourozieh; Abedi, 2013). This asymmetry in molecular size and interactions, exacerbated by temperature effects, promotes the formation of liquid-liquid and liquid-liquid-vapor transitions, where L_1 represents the CO_2-rich liquid phase and L_2 the hydrocarbon-rich phase.

5.3 Results of Thermodynamic Modeling

5.3.1 The Peng-Robinson modeling results for the binary system CO_2/decane

Figure 28 shows the Peng-Robinson modeling results for the binary system CO_2/decane, with experimental saturation pressure data overlaid at different CO_2 molar compositions as a function of temperature T = (283.15, 298.15, and 323.15) K. The continuous line represents the data calculated without correcting binary interaction parameters (k_{ij} equal to zero), where a significant deviation from the experimental values is observed. The dashed line, which more accurately follows the experimental points trend, corresponds to the data calculated with a temperature-dependent k_{ij}.

Figure 28 - Bubble pressure (P/MPa) for the system CO_2 + decane at different CO_2 molar compositions. Bubble point (circle, o); Peng-Robinson equation of state with k_{ij} dependent of the temperature (dashed lines, --); Peng-Robinson equation of state with k_{ij} equal to zero (continuous lines, —). The lines are differentiated by colors representing each temperature: 323.15 K (red, —), 298.15 K (blue, —), and 283.15 K (green, —).

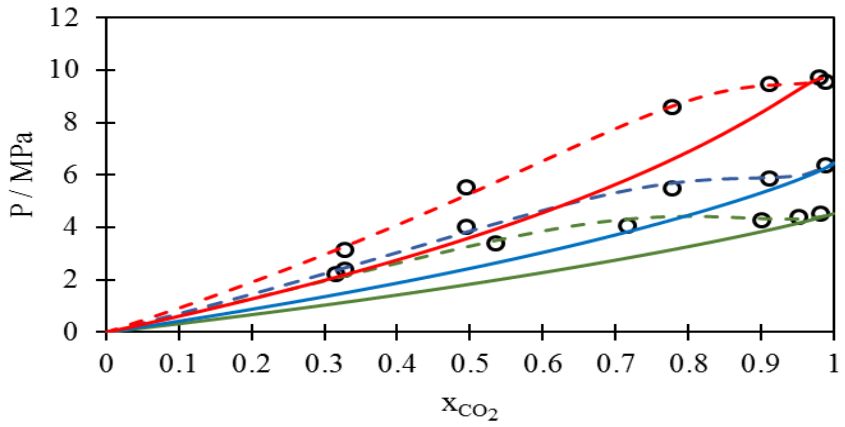

Source: Created by the author (2024).

5.3.2 Binary interaction coefficients kij for each temperature studied

To analyze the accuracy of the predictions made by the Peng-Robinson equation of state, the following statistical indicator expressed in Eq. 28 was used (Silva, Maxwell Risseli Laurentino da, 2022).

$$\%AARD = \frac{1}{N_p}\sum_{i}^{Np}\left|\frac{P_i^{cal} - P_i^{exp}}{P_i^{exp}}\right| \qquad (28)$$

Where *%AARD* is defined as the average absolute relative deviation, providing the statistical accuracy of the predictions. As expected, the deviation values increase significantly when the ternary system has a higher composition of hexadecane relative to decane and when working with overall compositions greater than 80% CO_2. A maximum value of 38.77% was found for the M-80 + CO_2 mixtures and a minimum value of 1.06% for the M-20 + CO_2 mixtures, where, in the latter case, the results successfully followed the observed experimental trend.

Table 12 shows the different binary interaction coefficients for each evaluated temperature for the CO_2 + n-$C_{10}H_{22}$ and CO_2 + n-$C_{16}H_{34}$ systems, as well as the value of k_{ij} equal to zero considered for the hydrocarbon/hydrocarbon binary interaction, i.e., n-$C_{10}H_{22}$/n-$C_{16}H_{34}$.

Table 12 - Binary interaction coefficients k_{ij} for each temperature studied.

k_{ij} (T = 283.15 K)	CO_2	n-$C_{10}H_{22}$	n-$C_{16}H_{34}$
CO_2	0	0.12279	0.11405
n-$C_{10}H_{22}$	0.12279	0	0
n-$C_{16}H_{34}$	0.11405	0	0
k_{ij} (T = 298.15 K)	CO_2	n-$C_{10}H_{22}$	n-$C_{16}H_{34}$
CO_2	0	0.10477	0.10910
n-$C_{10}H_{22}$	0.10477	0	0
n-$C_{16}H_{34}$	0.10910	0	0
k_{ij} (T = 323.15 K)	CO_2	n-$C_{10}H_{22}$	n-$C_{16}H_{34}$
CO_2	0	0.09670	0.10127
n-$C_{10}H_{22}$	0.09670	0	0
n-$C_{16}H_{34}$	0.10127	0	0

Source: Created by the author (2024).

Table 13 summarizes the maximum average relative deviations (%AARD) for the calculated data compared to the experimental points. It is possible to observe that the deviation strongly depends on the hexadecane composition. These deviations are mainly associated with the formation of polar dipoles at high pressure and the associative nature of the systems at high

CO_2 compositions, being categorized as complex diagrams in the Van Konynenburg classification (Van Konynenburg, P. H.; Scott R. L., 1980).

Table 13 - Average relative percentage deviations for the different systems studied.

	%AARD		
T/K	**283.15**	**298.15**	**323.15**
M-20 + CO_2	3.76	4.53	7.73
M-40 + CO_2	1.06	2.45	15.39
M-60 + CO_2	11.41	11.87	27.96
M-80 + CO_2	7.55	13.27	36.78

Source: Created by the author (2024).

The behavior of the modeled curve varies considerably with temperature, even though the temperature-dependent k_{ij} parameter was adjusted. This kind of result is expected because, as the CO_2 composition increases, the systems approach the critical state (or the point of continuity between the liquid and vapor phases). Additionally, it is considered that the PR equation of state has limited capacity to represent highly asymmetric systems, especially when using classical mixing rules and only the attractive binary interaction parameter (Cismondi Duarte *et al.*, 2014; Cismondi; Mollerup; Zabaloy, 2010; Yanes; Montel; Daridon, 2022)

5.3.3 Density inversion modeling

An additional test was performed for predicting density inversion phenomena observed. To do so, a series of flash calculations was performed for the CO_2 + M-60 and CO_2 + M-80 mixtures. The resulting density versus pressure graphs are shown in Figures 29 and 30, respectively. It can be observed a clearly phase density inversion when the pressure decreases for both systems at pressure condition near to 7.3 MPa. Although the PR-EoS is capable to predict the pressure condition when both fluid phases present a density inversion, a difference higher than 1 MPa was observed to the inversion experimentally observed.

Figure 29 - Density plotted as a function of pressure: M-60 + CO_2, dashed line (-) 0.898 and continuous line (—) 0.953 fraction molar of CO_2 in the global composition at 298.15 K.

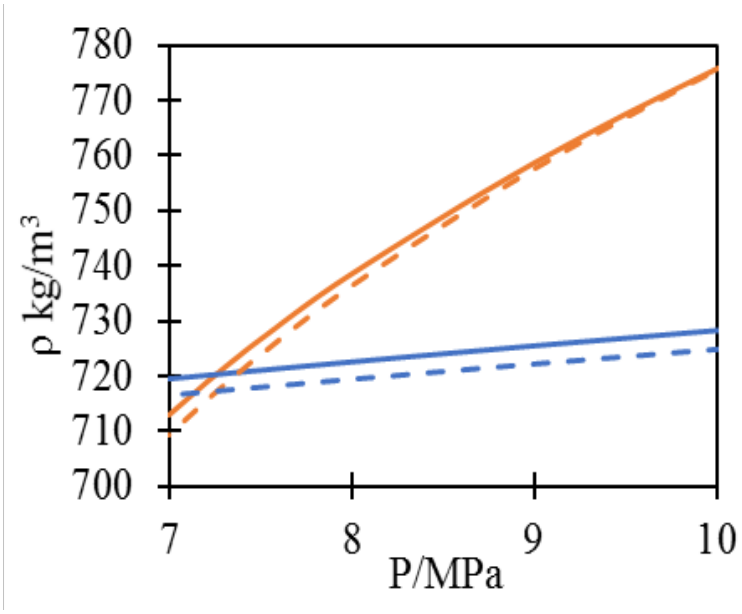

Source: Created by the author (2024).

Figure 30 - Density plotted as a function of pressure: M-80 + CO_2, dashed line (-) 0.9 and continuous line (—) 0.949 fraction molar of CO_2 in the global composition at 298.15 K.

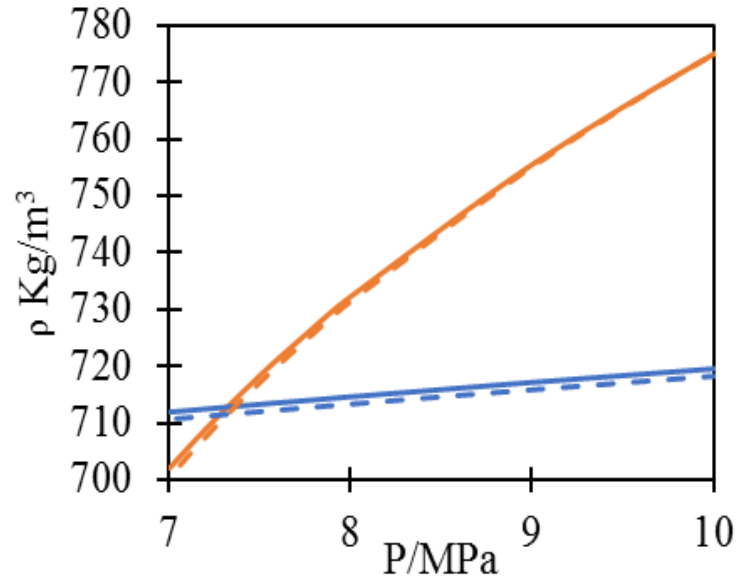

Source: Own work (2024).

6 CONCLUSIONS

The experimental phase behavior of the ternary systems CO_2 + decane + hexadecane was determined under subcritical (283.15 and 298.15 K) and supercritical (323.15 K) temperature conditions, covering a wide range of added gas compositions. The ternary system exhibited typical behavior for compositions with an 80/20 (decane/hexadecane) ratio. This means obtaining bubble points at temperatures of 283.15 and 298.15 K. And for the temperature of 323.15 K, bubble points are obtained and for CO_2 values greater than 95% in the global composition, dew points are obtained.

The addition of hexadecane to the system increased the saturation pressure for the same mole fraction of gas compared to the liquid mixture. This effect also created windows of immiscibility, evidenced by the appearance of a liquid-liquid phase. Furthermore, under conditions in which the composition of hexadecane exceeds that of decane, the phenomenon of barotropic inversion was observed. This phenomenon, characterized by a density inversion, is common in CO_2 + hexadecane binary systems at temperatures below the critical point of CO_2. Therefore, this complex behavior can be attributed to the presence of hexadecane in the mixture. These findings are essential to understanding the forces that drive interactions in mixtures and how these forces change with variations in pressure and temperature.

The thermodynamic modeling of the studied systems was performed using the Peng-Robinson equation of state, with temperature-dependent binary interaction parameters for CO_2/decane and CO_2/hexadecane. The model provided satisfactory results for compositions with low amounts of n-hexadecane and CO_2. However, for high CO_2 compositions (above 80%) and higher amounts of hexadecane compared to decane, the model was unable to identify liquid-liquid equilibrium, resulting in an infinite curve. This indicates that the model, using the binary interaction parameter values defined in the work, could not describe the conditions under which the system transitions from liquid to liquid-liquid and could only provide values for liquid-liquid-vapor.

REFERENCES

AL GHAFRI, Saif Z.; MAITLAND, Geoffrey C.; TRUSLER, J. P. Martin. Experimental and modeling study of the phase behavior of synthetic crude oil + CO2. **Fluid Phase Equilibria**, [*s. l.*], v. 365, p. 20–40, 2014.

AL GHAFRI, Saif. **Phase Behaviour and Physical Properties of Reservoir Fluids Under Addition of Carbon Dioxide**. 2013. - Imperial College London, London SW7 2AZ, United Kingdom, 2013.

AMBROSE, Douglas; TSONOPOULOS, Constantine. Vapor-Liquid Critical Properties of Elements and Compounds. 2. Normal Alkanes. **Journal of Chemical & Engineering Data**, [*s. l.*], v. 40, n. 3, p. 531–546, 1995.

AYALA H., Luis F.; MORGAN, Eugene C. Natural Gas Production Engineering. *In*: RIAZI, M. R. **Exploration and Production of Petroleum and Natural Gas**. [*S. l.*]: ASTM International100 Barr Harbor Drive, PO Box C700, West Conshohocken, PA 19428-2959, 2016. p. 395–428. Available at: https://asmedigitalcollection.asme.org/astm-ebooks/book/652/chapter/27758849/Natural-Gas-Production-Engineering.

BALBINOT FILHO, Clóvis A. *et al.* High-pressure phase equilibrium data of carbon dioxide/food-relevant systems (2011-2022): Experimental methods, multiphase behavior, thermodynamic modeling, and applications. **Fluid Phase Equilibria**, [*s. l.*], v. 572, p. 113851, 2023.

BELTRAO, Ricardo L. Carneiro *et al.* SS: Pre-salt Santos basin - Challenges and New Technologies for the Development of the Pre-salt Cluster, Santos Basin, Brazil. *In*: OFFSHORE TECHNOLOGY CONFERENCE, 2009, Houston, Texas. **All Days**. Houston, Texas: OTC, 2009. p. OTC-19880-MS. Available at: https://onepetro.org/OTCONF/proceedings/09OTC/All-09OTC/Houston,%20Texas/35954.

BLUMA, Martin; DEITERS, Ulrich K. A classification of phase diagrams of ternary fluid systems. **Physical Chemistry Chemical Physics**, [*s. l.*], v. 1, n. 18, p. 4307–4313, 1999.

BRAGA, Arthur J. O.; TAVARES, Frederico W.; NDIAYE, Papa M. A new high-pressure cell for equilibrium measurements of systems with fluid and solid phases. **The Journal of Supercritical Fluids**, [*s. l.*], v. 179, p. 105420, 2022.

BREMAN B. B. *et al.* Gas-Liquid Solubilities of Carbon Monoxide, Carbon Dioxide,Hydrogen, Water, 1-Alcohols (1 .ltoreq. n .ltoreq. 6), and n-Paraffins (2 .ltoreq. n .ltoreq. 6) in Hexadecane, Octacosane, 1-Hexadecanol, Phenanthrene, and Tetraethylene Glycol at Pressures up to 5.5 MPa and Temperatures from 293 to 553 K. **Journal of Chemical & Engineering Data**, [*s. l.*], 1994. Available at: https://pubs.acs.org/doi/10.1021/je00016a004.

BRUNNER, Gerd; TEICH, Jens; DOHRN, Ralf. Phase equilibria in systems containing hydrogen, carbon dioxide, water and hydrocarbons. **Fluid Phase Equilibria**, [*s. l.*], v. 100, p. 253–268, 1994.

CAMPBELL, Flake C. Ternary Phase Diagrams. *In*: PHASE DIAGRAMS: UNDERSTANDING THE BASICS. [*S. l.*]: ASM International, 2012. p. 381–388.

CHAROENSOMBUT-AMON, T.; MARTIN, Raymond J.; KOBAYASHI, Riki. Application of

a generalized multiproperty apparatus to measure phase equilibrium and vapor phase densities of supercritical carbon dioxide in n-hexadecane systems up to 26 MPa. **Fluid Phase Equilibria**, [*s. l.*], v. 31, n. 1, p. 89–104, 1986.

CHAROS, Georgios N. *et al.* Three-dimensional *PTx* phase diagrams through interactive computer graphics. **Fluid Phase Equilibria**, [*s. l.*], v. 23, n. 1, p. 59–78, 1985.

CHEN ROGER J. J.; CHAPPELEAR Patsy S.; KOBAYASHI Riki. Dew-point loci for methane-n-hexane and methane-n-heptane binary systems. **Journal of Chemical & Engineering Data**, [*s. l.*], 1976. Available at: https://pubs.acs.org/doi/10.1021/je60069a025. Acesso em: 29 jan. 2025.

CHOU, Grace F.; FORBERT, Rainald R.; PRAUSNITZ, John M. High-pressure vapor-liquid equilibria for carbon dioxide/n-decane, carbon dioxide/tetralin, and carbon dioxide/n-decane/tetralin at 71.1 and 104.4.degree. C. **Journal of Chemical & Engineering Data**, [*s. l.*], v. 35, n. 1, p. 26–29, 1990.

CHRISTOV, M.; DOHRN, R. **High-pressure fluid phase equilibria: Experimental methods and systems investigated (1994-1999)**. [*S. l.: s. n.*], 2002-. ISSN 03783812.v. 202

CISMONDI, Martín *et al.* Phase equilibria of CO 2 + n-alkane binary systems in wide ranges of conditions: Development of predictive correlations based on cubic mixing rules. **Industrial and Engineering Chemistry Research**, [*s. l.*], v. 51, n. 17, p. 6232–6250, 2012.

CISMONDI DUARTE, M. *et al.* High pressure phase behavior modeling of asymmetric alkane + alkane binary systems with the RKPR EOS. **Fluid Phase Equilibria**, [*s. l.*], v. 362, Special Issue on PPEPPD 2013, p. 125–135, 2014.

CISMONDI, Martín; MICHELSEN, Michael L. Global phase equilibrium calculations: Critical lines, critical end points and liquid–liquid–vapour equilibrium in binary mixtures. **The Journal of Supercritical Fluids**, [*s. l.*], v. 39, n. 3, p. 287–295, 2007.

CISMONDI, Martín; MOLLERUP, Jørgen M.; ZABALOY, Marcelo S. Equation of state modeling of the phase equilibria of asymmetric CO2 + n-alkane binary systems using mixing rules cubic with respect to mole fraction. **The Journal of Supercritical Fluids**, [*s. l.*], v. 55, n. 2, 100th year Anniversary of van der Waals' Nobel Lecture, p. 671–681, 2010.

COQUELET, Christophe *et al.* Experimental Determination of Thermophysical Properties of Working Fluids for ORC Applications. *In*: ORGANIC RANKINE CYCLES FOR WASTE HEAT RECOVERY - ANALYSIS AND APPLICATIONS. [*S. l.*]: IntechOpen, 2019. Available at: https://www.intechopen.com/chapters/67909.

CREEK, J. L.; SHEFFIELD, J. M. Phase Behavior, Fluid Properties, and Displacement Characteristics of Permian Basin Reservoir Fluid/CO2 Systems. **SPE Reservoir Engineering**, [*s. l.*], v. 8, n. 01, p. 34–42, 1993.

DA COSTA, Moacir Frutuoso Leal *et al.* Phase behavior of supercritical CO2 + nonionic ethoxylated surfactants + methanol: Experimental data and modeling with PC-SAFT equation of state. **Fluid Phase Equilibria**, [*s. l.*], v. 583, p. 114130, 2024.

DARIDON, Jean-Luc *et al.* Fluid-fluid and fluid-solid phase equilibria in carbon dioxide + waxy systems 1. CO2 + n-C17. **Fluid Phase Equilibria**, [*s. l.*], v. 538, p. 113023,

2021.

DAVENPORT, A. J.; ROWLINSON, J. S. The solubility of hydrocarbons in liquid methane. **Transactions of the Faraday Society**, [*s. l.*], v. 59, n. 0, p. 78–84, 1963.

DAVENPORT, A. J.; ROWLINSON, J. S.; SAVILLE, G. Solutions of three hydrocarbons in liquid methane. **Transactions of the Faraday Society**, [*s. l.*], v. 62, p. 322, 1966.

DOHRN, Ralf *et al.* High-pressure fluid-phase equilibria: Experimental methods, developments and systems investigated (2013–2016). **Fluid Phase Equilibria**, [*s. l.*], v. 579, p. 113978, 2024.

DOHRN, Ralf; BRUNNER, Gerd. High-pressure fluid-phase equilibria: Experimental methods and systems investigated (1988–1993). **Fluid Phase Equilibria**, [*s. l.*], v. 106, n. 1, p. 213–282, 1995.

DOHRN, Ralf; PEPER, Stephanie; FONSECA, José M. S. High-pressure fluid-phase equilibria: Experimental methods and systems investigated (2000–2004). **Fluid Phase Equilibria**, [*s. l.*], v. 288, n. 1, p. 1–54, 2010.

D'SOUZA, Rupert; PATRICK, Jennie R.; TEJA, Amyn S. High pressure phase equilibria in the carbon dioxide - n-Hexadecane and carbon dioxide — water systems. **The Canadian Journal of Chemical Engineering**, [*s. l.*], v. 66, n. 2, p. 319–323, 1988.

EDWARDS, Ylva; ISACSSON, Ulf. Wax in Bitumen. Part 1—Classifications and General Aspects. **Road Materials and Pavement Design**, [*s. l.*], 2005. Available at: https://www.tandfonline.com/doi/abs/10.1080/14680629.2005.9690009.

ELIAS, A.; TREVISAN, Osvair V. An experimental investigation on phase behavior of a light oil and CO2. **Journal of Petroleum Science and Engineering**, [*s. l.*], v. 145, p. 22–33, 2016.

ENIOLORUNDA, Oluwakemi V.; CHAPOY, Antonin; BURGASS, Rod. Phase Equilibria of Waxy Live Oil Systems Containing CO2: Experimental Measurements and Thermodynamic Modeling. **Energy & Fuels**, [*s. l.*], v. 35, n. 5, p. 3731–3741, 2021.

ESTRERA, Susana S.; LUKS, Kraemer D. Liquid-liquid-vapor equilibria behavior of certain ethane + n-paraffin mixtures. **Journal of Chemical & Engineering Data**, [*s. l.*], v. 32, 2, p. 201–204, 1987.

FALL, David J.; FALL, Jaimie L.; LUKS, Kraemer D. Liquid-liquid-vapor immiscibility limits in carbon dioxide + n-paraffin mixtures. **Journal of Chemical & Engineering Data**, [*s. l.*], v. 30, n. 1, p. 82–88, 1985.

FALL, David J.; LUKS, Kraemer D. Phase equilibria behavior of the systems carbon dioxide + n-dotriacontane and carbon dioxide + n-docosane. **Journal of Chemical & Engineering Data**, [*s. l.*], v. 29, n. 4, p. 413–417, 1984.

FELE ŽILNIK, Ljudmila *et al.* Phase-equilibrium measurements with a novel multi-purpose high-pressure view cell: CO2 + n-decane and CO2 + toluene. **Fluid Phase Equilibria**, [*s. l.*], v. 419, p. 31–38, 2016.

FERREIRA, F. A. V. *et al.* Characterization, Pressure–Volume–Temperature Properties, and

Phase Behavior of a Condensate Gas and Crude Oil. **Energy & Fuels**, [*s. l.*], v. 32, n. 4, p. 5643–5649, 2018.

FLORES, Mauricio E. *et al.* A topological approach to mass barotropic phenomena in asymmetric mixtures. **Fluid Phase Equilibria**, [*s. l.*], v. 313, p. 171–181, 2012.

FONSECA, José M. S.; DOHRN, Ralf; PEPER, Stephanie. High-pressure fluid-phase equilibria: Experimental methods and systems investigated (2005–2008). **Fluid Phase Equilibria**, [*s. l.*], v. 300, n. 1, p. 1–69, 2011.

FORNARI, Rosa E.; ALESSI, Paolo; KIKIC, Ireneo. High pressure fluid phase equilibria: experimental methods and systems investigated (1978–1987). **Fluid Phase Equilibria**, [*s. l.*], v. 57, n. 1, p. 1–33, 1990.

FORTE, Esther; GALINDO, Amparo; TRUSLER, J. P. Martin. Experimental and molecular modeling study of the three-phase behavior of (n-decane + carbon dioxide + water) at reservoir conditions. **The Journal of Physical Chemistry. B**, [*s. l.*], v. 115, n. 49, p. 14591–14609, 2011.

FRANÇA, Daniela *et al.* Speciation and quantification of high molecular weight paraffins in Brazilian whole crude oils using high-temperature comprehensive two-dimensional gas chromatography. **Fuel**, [*s. l.*], v. 234, p. 1154–1164, 2018.

FRANCIS, Alfred W. Ternary Systems of Liquid Carbon Dioxide. **The Journal of Physical Chemistry**, [*s. l.*], v. 58, p. 1099–1114, 1954.

GAO, Guanghua *et al.* A simple correlation to evaluate binary interaction parameters of the Peng-Robinson equation of state: binary light hydrocarbon systems. **Fluid Phase Equilibria**, [*s. l.*], v. 74, p. 85–93, 1992.

GIBBS, J. Willard. **On the equilibrium of heterogeneous substances : first [-second] part pt. 1**. [*S. l.*]: Published by the Academy, 1874.

HAN, Haishui *et al.* Dissolving capacity and volume expansion of carbon dioxide in chain n-alkanes. **Petroleum Exploration and Development**, [*s. l.*], v. 42, n. 1, p. 97–103, 2015.

HENDERSON, N. *et al.* Modeling and Analysis of the Isothermal Flash Problem and Its Calculation with the Simulated Annealing Algorithm. **Industrial & Engineering Chemistry Research**, [*s. l.*], v. 40, n. 25, p. 6028–6038, 2001.

HIRSCHBERG, A. *et al.* Influence of Temperature and Pressure on Asphaltene Flocculation. **Society of Petroleum Engineers journal**, [*s. l.*], v. 24, n. 3, p. 283–293, 1984.

HÖLSCHER, I. F.; SPEE, M.; SCHNEIDER, G. M. Fluid-phase equilibria of binary and ternary mixtures of CO2 with hexadecane, 1-dodecanol, 1-hexadecanol and 2-ethoxy-ethanol at 333.2 and 393.2 K and at pressures up to 33 MPa. **Fluid Phase Equilibria**, [*s. l.*], v. 49, p. 103–113, 1989.

HONG, Seung Pyo; PATTON, Christi L.; LUKS, Kraemer D. Multiphase equilibrium behavior of the mixture carbon dioxide + ethane + methanol. **Journal of Chemical & Engineering Data**, [*s. l.*], v. 39, n. 1, p. 90–94, 1994.

HOTTOVY, John D.; LUKS, Kraemer D.; KOHN, James P. Three-phase liquid-liquid-vapor

equilibriums behavior of certain binary carbon dioxide-n-paraffin systems. **Journal of Chemical & Engineering Data**, [*s. l.*], v. 26, n. 3, p. 256–258, 1981.

INOMATA, Hiroshi *et al.* Measurement of vapor-liquid equilibria at elevated temperatures and pressures using a flow type apparatus. **JOURNAL OF CHEMICAL ENGINEERING OF JAPAN**, [*s. l.*], v. 19, n. 5, p. 386–391, 1986.

JANGKAMOLKULCHAI, Adisak; ARBUCKLE, Melanie M.; LUKS, Kraemer D. Liquid—liquid—vapor phase equilibria behavior of certain binary ethane + n-alkylbenzene mixtures. **Fluid Phase Equilibria**, [*s. l.*], v. 40, n. 3, p. 235–245, 1988.

JANGKAMOLKULCHAI, Adisak; LUKS, Kraemer D. Partial miscibility behavior of the methane + ethane + n-docosane and the methane + ethane + n-tetradecylbenzene ternary mixtures. **Journal of Chemical & Engineering Data**, [*s. l.*], v. 34, n. 1, p. 92–99, 1989.

JIMÉNEZ-GALLEGOS, R.; GALICIA-LUNA, L. A.; ELIZALDE-SOLIS, O. Experimental Vapor−Liquid Equilibria for the Carbon Dioxide + Octane and Carbon Dioxide + Decane Systems. **Journal of Chemical & Engineering Data**, [*s. l.*], v. 51, n. 5, p. 1624–1628, 2006.

JUNTARACHAT, Niramol *et al.* Validation of a new apparatus using the dynamic method for determining the critical properties of binary mixtures containing CO2 and a n-alkane. **Fluid Phase Equilibria**, [*s. l.*], v. 325, p. 66–70, 2012.

KANDIL, Mohamed E.; AL-SAIFI, Nayef M.; SULTAN, Abdullah S. Simulation and measurements of volumetric and phase behavior of carbon dioxide + higher alkanes at high pressure: CO 2 + n -decane at temperatures (313–410) K and pressures up to 76 MPa. **International Journal of Greenhouse Gas Control**, [*s. l.*], v. 53, p. 198–206, 2016.

KARIZNOVI, Mohammad; NOUROZIEH, Hossein; ABEDI, Jalal. Phase composition and saturated liquid properties in binary and ternary systems containing carbon dioxide, n-decane, and n-tetradecane. **The Journal of Chemical Thermodynamics**, [*s. l.*], v. 57, p. 189–196, 2013.

KNUDSEN, Kim; POULSEN, Thomas. **SPECS V5.6x.** [*S. l.: s. n.*], 2009.

KONTOGEORGIS, Georgios M.; FOLAS, Georgios K. Thermodynamic Models for Industrial Applications: From Classical and Advanced Mixing Rules to Association Theories. **Thermodynamic Models for Industrial Applications: From Classical and Advanced Mixing Rules to Association Theories**, [*s. l.*], p. 1–692, 2009.

KORDIKOWSKI, Andreas; SCHNEIDER, Gerhard M. Fluid phase equilibria of binary and ternary mixtures of supercritical carbon dioxide with low-volatility organic substances up to 100 MPa and 393 K: c. **Fluid Phase Equilibria**, [*s. l.*], v. 90, n. 1, p. 149–162, 1993.

KORETSKY, Milo D. **Engineering and chemical thermodynamics**. 2nd editioned. Hoboken, NJ: Wiley, 2013.

KUKARNI, Ajit A. *et al.* Phase-equilbriums behavior of system carbon dioxide-n-decane at low temperatures. **Journal of Chemical & Engineering Data**, [*s. l.*], v. 19, n. 1, p. 92–94, 1974.

LATSKY, Carla; CORDEIRO, Brandon; SCHWARZ, Cara E. High pressure bubble- and dew-point data for systems containing CO2 with 1-decanol and n-hexadecane. **Fluid Phase Equilibria**, [*s. l.*], v. 521, p. 112702, 2020.

LEAL, Monique F. **Experimental determination and thermodynamic modeling of phase equilibria in systems with CO2, n-hexane, n-hexadecane, and tetralin**. 2015. Masters Dissertation - Universidade do Estado do Rio de Janeiro, Rio de Janeiro, Brazil, 2015. Available at: http://www.bdtd.uerj.br/handle/1/12026.

LEWIS, Gilbert Newton. The Law of Physico-Chemical Change. **Proceedings of the American Academy of Arts and Sciences**, [*s. l.*], v. 37, n. 3, p. 49, 1901.

LIN, Yueh-Neu; HWANG, Shuen-Cheng; KOBAYASHI, Riki. Vapor-liquid equilibrium of the methane-toluene system at low temperatures. **Journal of Chemical & Engineering Data**, [*s. l.*], v. 23, n. 3, p. 231–234, 1978.

LÓPEZ, Jimmy A.; TREJOS, Victor M.; CARDONA, Carlos A. Objective functions analysis in the minimization of binary VLE data for asymmetric mixtures at high pressures. **Fluid Phase Equilibria**, [*s. l.*], v. 248, n. 2, p. 147–157, 2006.

LUCAS, Marcos A. *et al.* Use of real crude oil fractions to describe the high pressure phase behavior of crude oil in carbon dioxide. **The Journal of Supercritical Fluids**, [*s. l.*], v. 118, p. 140–147, 2016.

MAINWARING, David E.; SADUS, Richard J.; YOUNG, Colin L. Prediction of binary and ternary critical properties using deiters' equation, hard sphere and hard convex body equations of state. **Fluid Phase Equilibria**, [*s. l.*], v. 42, Third International IUPAC Workshop on Vapor\3-Liquid Equilibria in 1-Alkanol+n-Alkane Mixtures, p. 85–103, 1988.

MCCAIN, William D. **The properties of petroleum fluids**. Third editioned. Tulsa, Oklahoma: PennWell, 2017.

MEDEIROS, Hugo Andersson Dantas *et al.* Fluid phase equilibria of Brazilian presalt crude oil – CO2 systems at high pressure and high temperature. **The Journal of Supercritical Fluids**, [*s. l.*], v. 201, p. 106033, 2023.

MICHELSEN, Michael L. The isothermal flash problem. Part I. Stability. **Fluid Phase Equilibria**, [*s. l.*], v. 9, n. 1, p. 1–19, 1982a.

MICHELSEN, Michael L. The isothermal flash problem. Part II. Phase-split calculation. **Fluid Phase Equilibria**, [*s. l.*], v. 9, n. 1, p. 21–40, 1982b.

NAGARAJAN, N.; ROBINSON, R. L. Equilibrium phase compositions, phase densities, and interfacial tensions for carbon dioxide + hydrocarbon systems. 2. Carbon dioxide + n-decane. **Journal of Chemical & Engineering Data**, [*s. l.*], v. 31, n. 2, p. 168–171, 1986.

NASCIMENTO, Fábio P. *et al.* Phase behavior of CO2/toluene, CO2/n-decane and CO2/toluene/n-decane: Experimental measurements and thermodynamic modeling with SAFT-VR Mie equation of state. **The Journal of Supercritical Fluids**, [*s. l.*], v. 154, p. 104634, 2019.

NGHIEM, L. X.; LI, Y. K. Effect of Phase Behavior on CO2 Displacement Efficiency at Low Temperatures: Model Studies With an Equation of State. **SPE Reservoir Engineering**, [*s. l.*], v. 1, n. 04, p. 414–422, 1986.

NIEUWOUDT, I; DU RAND, M. Measurement of phase equilibria of supercritical carbon dioxide and paraffins. **The Journal of Supercritical Fluids**, [*s. l.*], v. 22, n. 3, p. 185–199, 2002.

ORR, F. M.; JENSEN, C. M. Interpretation of Pressure-Composition Phase Diagrams for CO2/Crude-Oil Systems. **Society of Petroleum Engineers Journal**, [*s. l.*], v. 24, n. 05, p. 485–497, 1984.

OTT, J. Bevan; BOERIO-GOATES, Juliana. **Chemical thermodynamics: advanced applications**. London, UK San Diego, Calif: Academic Press, 2000.

PEDERSEN, Karen Schou; THOMASSEN, Per; FREDENSLUND, Aage. Thermodynamics of petroleum mixtures containing heavy hydrocarbons. 3. Efficient flash calculation procedures using the SRK equation of state. **Industrial & Engineering Chemistry Process Design and Development**, [*s. l.*], v. 24, n. 4, p. 948–954, 1985.

PENG, Ding-Yu; ROBINSON, Donald B. A New Two-Constant Equation of State. **Industrial & Engineering Chemistry Fundamentals**, [*s. l.*], v. 15, n. 1, p. 59–64, 1976.

PETERS, C. J. *et al.* The search for tricriticality in binary mixtures of near-critical propane and normal paraffins. **Fluid Phase Equilibria**, [*s. l.*], v. 51, n. C, p. 339–351, 1989.

POLISHUK, Ilya; WISNIAK, Jaime; SEGURA, Hugo. Simultaneous prediction of the critical and sub-critical phase behavior in mixtures using equation of state I. Carbon dioxide-alkanols. **Chemical Engineering Science**, [*s. l.*], v. 56, n. 23, p. 6485–6510, 2001.

PRIVAT, Romain; JAUBERT, Jean-Noël. Classification of global fluid-phase equilibrium behaviors in binary systems. **Chemical Engineering Research and Design**, [*s. l.*], v. 91, n. 10, p. 1807–1839, 2013.

QUIÑONES-CISNEROS, Sergio E. Barotropic phenomena in complex phase behaviour. **Phys. Chem. Chem. Phys.**, [*s. l.*], v. 6, n. 9, p. 2307–2313, 2004.

QUIÑONES-CISNEROS, Sergio E. Phase and critical behavior in type III phase diagrams. **Fluid Phase Equilibria**, [*s. l.*], v. 134, n. 1–2, p. 103–112, 1997.

QUINTEROS-LAMA, Héctor *et al.* Barotropic phenomena in binary mixtures. **Fluid Phase Equilibria**, [*s. l.*], v. 394, p. 175–185, 2015.

RATHMELL, J.J.; STALKUP, F.I.; HASSINGER, R.C. A Laboratory Investigation of Miscible Displacement by Carbon Dioxide. [*s. l.*], 1971.

REAMER, H. H.; SAGE, B. H. Phase Equilibria in Hydrocarbon Systems. Volumetric and Phase Behavior of the n-Decane-CO2 System. **Journal of Chemical & Engineering Data**, [*s. l.*], v. 8, n. 4, p. 508–513, 1963.

REN, Wei; SCURTO, Aaron M. High-pressure phase equilibria with compressed gases. **Review of Scientific Instruments**, [*s. l.*], v. 78, n. 12, p. 125104, 2007.

ROMERO YANES, Jose F. *et al.* Measurement of Fluid Phase Equilibria for High Gas Ratio Mixtures of Carbon Dioxide, Methane, and Brazilian Presalt Crude Oil. **Journal of Chemical & Engineering Data**, [*s. l.*], v. 66, n. 3, p. 1356–1366, 2021.

ROMERO YANES, Jose F. *et al.* Study of Liquid–Liquid and Liquid–Liquid–Vapor Equilibria for Crude Oil Mixtures with Carbon Dioxide and Methane Using Short-Wave Infrared Imaging: Experimental and Thermodynamic Modeling. **Energy & Fuels**, [*s. l.*], v. 34, n. 11, p. 14109–

14123, 2020.

SANDLER, Stanley I. **Chemical, biochemical, and engineering thermodynamics**. Fifth editioned. Hoboken, NJ: Wiley, 2017.

SAVONINA, E. Yu.; PANYUKOVA, D. I. State of the Art and Prospects for the Development of Methods for Determining the Group Hydrocarbon Composition (SARA Composition) of Crude Oil and Petroleum Products. **Russian Journal of Applied Chemistry**, [*s. l.*], v. 96, n. 5, p. 503–524, 2023.

SCHNEIDER, G. *et al.* Phasengleichgewichte und kritische Erscheinungen in binären Mischsystemen bis 1500 bar, CO_2 mit n-Octan, n-Undecan, n-Tridecan und n-Hexadecan. **Chemie Ingenieur Technik**, [*s. l.*], v. 39, n. 11, p. 649–656, 1967.

SCHNEIDER, Gerhard M.; SCHEIDGEN, Arndt L.; KLANTE, Dirk. Complex Phase Equilibrium Phenomena in Fluid Mixtures up to 2 GPa−Cosolvency, Holes, Windows, Closed Loops, High-Pressure Immiscibility, Barotropy, and Related Effects. **Industrial & Engineering Chemistry Research**, [*s. l.*], v. 39, n. 12, p. 4476–4480, 2000.

SEBASTIAN, Herbert M. *et al.* Vapor-liquid equilibrium in binary mixtures of carbon dioxide + n-decane and carbon dioxide + n-hexadecane. **Journal of Chemical & Engineering Data**, [*s. l.*], v. 25, n. 2, p. 138–140, 1980.

SHAVER, R.D; ROBINSON, R.L; GASEM, K.A.M. An automated apparatus for equilibrium phase compositions, densities, and interfacial tensions: data for carbon dioxide + decane. **Fluid Phase Equilibria**, [*s. l.*], v. 179, n. 1–2, p. 43–66, 2001.

DA SILVA, Maxwell R. L. **Estudo do Comportamento de Fase e Volumétrico do Sistema Dióxido de Carbono + n-Hexadecano + n-Butil Ciclohexano a Altas Temperaturas e Pressões**. 2022. Masters Dissertation - Universidade Federal do Ceará, Fortaleza, Brazil, 2022. Available at: http://www.repositorio.ufc.br/handle/riufc/65953.

SIMONCELLI, Ana P.P. *et al.* Phase behavior of systems with high CO2 content: Experiments and thermodynamic modeling. **Fluid Phase Equilibria**, [*s. l.*], v. 515, p. 112574, 2020.

SPECOVIUS, Juergen *et al.* Tricritical phenomena in quasi-binary mixtures of hydrocarbons. 2. Binary ethane systems. **The Journal of Physical Chemistry**, [*s. l.*], v. 85, n. 16, p. 2313–2316, 1981.

SPEE, M.; SCHNEIDER, G.M. Fluid phase equilibrium studies on binary and ternary mixtures of carbon dioxide with hexadecane, 1-dodecanol, 1,8-octanediol and dotriacontane at 393.2 K and at pressures up to 100 MPa. **Fluid Phase Equilibria**, [*s. l.*], v. 65, p. 263–274, 1991.

TARDÓN, María José *et al.* Molar isopycnicity in heterogeneous binary mixtures. **Fluid Phase Equilibria**, [*s. l.*], v. 336, p. 84–97, 2012.

TAYLOR, B.; KUYATT, C. **Guidelines for Evaluating and Expressing the Uncertainty of NIST Measurement Results**. Gaithersburg, MD: National Institute of Standards and Technology (NIST), 1994. NIST Technical Notes. Available at: https://nvlpubs.nist.gov/nistpubs/legacy/tn/nbstechnicalnote1297.pdf.

TSUJI, Tomoya *et al.* Measurements of bubble point pressure for CO2 + decane and CO2 +

lubricating oil. **Fluid Phase Equilibria**, [*s. l.*], v. 219, n. 1, p. 87–92, 2004.

VALERO, Chacón; MARIA, Angélica. **Study of phase and volumetric behavior of hydrocarbons and carbon dioxide ternary mixtures under high-temperature and high-pressure conditions**. 2020. Masters Dissertation, [*s. l.*], 2020. Available at: http://repositorio.ufc.br/handle/riufc/51536.

VAN DER STEEN, J.; DE LOOS, Th.W.; DE SWAAN ARONS, J. The volumetric analysis and prediction of liquid-liquid-vapor equilibria in certain carbon dioxide + n-alkane systems. **Fluid Phase Equilibria**, [*s. l.*], v. 51, p. 353–367, 1989.

VAN KONYNENBURG, P. H.; SCOTT R. L. Critical lines and phase equilibria in binary van der Waals mixtures. **Philosophical Transactions of the Royal Society of London. Series A, Mathematical and Physical Sciences**, [*s. l.*], v. 298, n. 1442, p. 495–540, 1980.

VAN PELT Arnold F. Critical phenomena in binary fluid mixtures: classification of phase equilibria with the simplified-perturbed-hard-chain theory. *In*: **Anais**. [*S. l.: s. n.*], 1992. Available at: https://api.semanticscholar.org/CorpusID:93955718.

VANINI, Gabriela *et al.* Analytical advanced techniques in the molecular-level characterization of Brazilian crude oils. **Microchemical Journal**, [*s. l.*], v. 137, p. 111–118, 2018.

VENTER, M.J. *et al.* Phase equilibria and physical properties of CO2-saturated cocoa butter mixtures at elevated pressures. **The Journal of Supercritical Fluids**, [*s. l.*], v. 41, n. 2, p. 195–203, 2007.

WANG, Quan-De *et al.* Systematic analysis and reduction of combustion mechanisms for ignition of multi-component kerosene surrogate. **Proceedings of the Combustion Institute**, [*s. l.*], v. 34, n. 1, p. 187–195, 2013.

YANES, Jose F. R.; MONTEL, F.; DARIDON, J.L. Fluid phase equilibria in asymmetric model systems. Part II: CO2 + 2,2,4,4,6,8,8-heptamethylnonane. **The Journal of Supercritical Fluids**, [*s. l.*], v. 189, p. 105721, 2022.

YANG, Zihao *et al.* Dispersion Property of CO_2 in Oil. 2: Volume Expansion of CO_2 + Organic Liquid at Near-Critical and Supercritical Conditions of CO_2. **Journal of Chemical & Engineering Data**, [*s. l.*], v. 57, n. 4, p. 1305–1311, 2012.

ZAMUDIO, M.; SCHWARZ, C.E.; KNOETZE, J.H. Phase equilibria of branched isomers of C10-alcohols and C10-alkanes in supercritical carbon dioxide. **The Journal of Supercritical Fluids**, [*s. l.*], v. 59, p. 14–26, 2011.